Monthly Notices
of the
ROYAL ASTRONOMICAL SOCIETY

Mon. Not. R. Astron. Soc. **426,** 1767–1781 (2012) doi:10.1111/j.1365-2966.2012.21766.x

The *Gaia* spectrophotometric standard stars survey – I. Preliminary results★

E. Pancino,[1]† G. Altavilla,[1] S. Marinoni,[1,2,3] G. Cocozza,[1] J. M. Carrasco,[4] M. Bellazzini,[1] A. Bragaglia,[1] L. Federici,[1] E. Rossetti,[5] C. Cacciari,[1] L. Balaguer Núñez,[4] A. Castro,[6] F. Figueras,[4] F. Fusi Pecci,[1] S. Galleti,[1] M. Gebran,[7] C. Jordi,[4] C. Lardo,[5] E. Masana,[4] M. Monguió,[4] P. Montegriffo,[1] S. Ragaini,[1] W. Schuster,[6] S. Trager,[8] F. Vilardell[9] and H. Voss[4]

[1]*Osservatorio Astronomico di Bologna, INAF, Via C. Ranzani, 1, I-40127 Bologna, Italy*
[2]*Osservatorio Astronomico di Roma, INAF, Via di Frascati, 33, I-00040 Monte Porzio Catone, Italy*
[3]*ASI Science Data Center, c/o ESA-ESRIN, Via Galileo Galilei, s/n, I-00044 Frascati, Italy*
[4]*Departament d'Astronomia i Meteorologia, Institut del Ciènces del Cosmos (ICC), Universitat de Barcelona (IEEC-UB), c/ Martí i Franquès, 1, 08028 Barcelona, Spain*
[5]*Dipartimento di Astronomia, Università di Bologna, Via C. Ranzani, 1, I-40127 Bologna, Italy*
[6]*Observatorio Astronómico Nacional, Universidad Nacional Autónoma de México, Apartado Postal 877, C. P. 22800 Ensenada, BC, Mexico*
[7]*Department of Physics and Astronomy, Notre Dame University Louiaze, PO Box 72, Zouk Mikael, Zouk Mosbeh, Lebanon*
[8]*Kapteyn Institute, University of Groningen, PO Box 800, 9700 AV Groningen, the Netherlands*
[9]*Institut d'Estudis Espacial de Catalunya, Edifici Nexus, c/ Capitá, 2-4, desp. 201, E-08034 Barcelona, Spain*

Accepted 2012 July 20. Received 2012 July 20; in original form 2012 June 22

ABSTRACT

We describe two ground-based observing campaigns aimed at building a grid of approximately 200 spectrophotometric standard stars (SPSS), with an internal $\simeq$1 per cent precision and tied to Vega within $\simeq$3 per cent, for the absolute flux calibration of data gathered by *Gaia*, the European Space Agency (ESA) astrometric mission. The criteria for the selection and a list of candidates are presented, together with a description of the survey strategy and the adopted data analysis methods. We also discuss a short list of notable rejected SPSS candidates and difficult cases, based on identification problems, literature discordant data, visual companions and variability. In fact, all candidates are also monitored for constancy (within $\pm$5 mmag, approximately). In particular, we report on a CALSPEC standard, 1740346, that we found to be a δ Scuti variable during our short-term monitoring (1–2 h) campaign.

Key words: techniques: photometric – techniques: spectroscopic – catalogues – stars: variables: δ Scuti.

1 INTRODUCTION

Gaia is a European Space Agency (ESA) all-sky astrometric, photometric and spectroscopic survey mission aimed at measuring parallaxes, proper motions, radial velocities and astrophysical parameters of $\simeq 10^9$ stars ($\simeq$1 per cent of the Galactic stellar population) down to magnitude $G \simeq 20$,[1] corresponding to $V \simeq$ 20–25 mag, depending on spectral type.

The astrometric accuracy is expected to be 5–14 μ as for bright stars ($V < 12$ mag), and to reach $\simeq$300 μ as down to $V \simeq 20$ mag. Radial velocities will be measured for stars brighter than $V \simeq 17$ mag, depending on spectral type, and their precision will range from 1 km s^{-1} for the bright stars down to 15–20 km s^{-1} for the faintest stars, bluer stars having higher uncertainties. The updated science performances of *Gaia* can be found on the *Gaia* ESA web page.[2]

The expected launch will be in 2013 August, from the ESA launch site at Kourou in French Guiana. *Gaia* will operate for approximately 5 years, with a possible 1 year extension, and the final catalogue is expected to be published 3 years after mission completion, while a set of intermediate releases is presently being defined.

★ Based on data obtained within the *Gaia* Data Processing and Analysis Consortium (DPAC) – and coordinated by the Ground-based Observations for *Gaia* (GBOG) working group – at various telescopes; see acknowledgments.

†E-mail: elena.pancino@oabo.inaf.it

[1] The *Gaia G* band is the unfiltered broad-band defined by the instrumental response curve, see also Fig. 1, extracted from Jordi et al. (2010).

[2] http://www.rssd.esa.int/index.php?project=GAIA&page=index

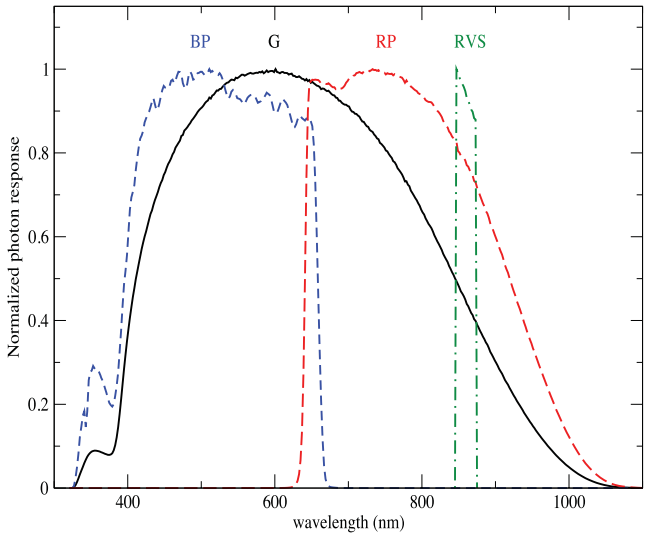

Figure 1. The photon response functions of the *Gaia G*, BP, RP and RVS passbands.

Although the primary scientific goal of *Gaia* is the characterization of the Milky Way, its scientific impact will range from Solar system studies to distant quasars, from unresolved galaxies to binaries, from supernovae to microlensing events, from fundamental physics to stellar variability. The wide variety of scientific topics is illustrated by almost 900 papers in Astrophysics Data System (ADS, of which more than 200 refereed) to date, on a diversity of subjects, from the description of various mission components (including software, pipelines and data treatment philosophy) to simulations of the expected scientific harvest in many diverse areas. Some papers summarize the expected science results (see e.g. Mignard 2005), but no single paper can be complete in this respect, given the huge range of possibilities opened by *Gaia*.

Three main instruments can be found on-board *Gaia*: the Astrometric Field (AF), consisting of 62 CCDs illuminated with white light, which will provide astrometric measurements and integrated *Gaia G*-band magnitudes (hereafter G); the Blue Photometer (BP) and Red Photometer (RP), consisting of two strips of seven CCDs each and providing prism dispersed, slitless spectra at a resolution of $R = \lambda/\delta\lambda \simeq 20$–$100$, covering the passbands shown in Fig. 1 and also providing integrated BP and RP magnitudes (hereafter $G_{\rm BP}$ and $G_{\rm RP}$) and the $G_{\rm BP} - G_{\rm RP}$ colour, which will be fundamental for chromaticity corrections of the astrometric measurements; and the Radial Velocity Spectrograph (RVS), providing $R \simeq 11\,000$ spectra in the calcium triplet region (8470–8740 Å) projected on to 12 CCDs. The mission output will thus be accurate positions, proper motions and parallaxes, low-resolution BP/RP spectra, integrated G, $G_{\rm BP}$ and $G_{\rm RP}$ magnitudes and the $G_{\rm BP} - G_{\rm RP}$ colour, plus medium-resolution RVS spectra and radial velocities for stars brighter than $V \simeq 17$ mag. A classification of all observed objects will be performed on the basis of BP/RP and RVS spectra and – when possible – their parametrization will be performed as well, which for stars will provide $T_{\rm eff}$, $\log g$, $E(B-V)$, [Fe/H] and [α/Fe].

Although *Gaia* is in principle a self-calibrating mission, some *Gaia* measurements need to be tied to existing absolute reference systems, and many *Gaia* algorithms need to be trained. Thus, extensive theoretical computations and observing campaigns are being carried out. To make a few examples, radial velocity standards that are stable to 1 km s^{-1} are being obtained (Crifo et al. 2010), extended libraries of observed and theoretical spectra (Tsalmantza & Bailer-Jones 2009; Sordo et al. 2010; Tsalmantza et al. 2012)[3] are being established and the ecliptic poles – that will be repeatedly observed in the initial calibration phase of *Gaia* observations – are being observed to produce catalogues of magnitudes and high-resolution spectra (Altman & Bastian 2009). Also, the selection and analysis of reference stars (and galaxies, quasars, asteroids, Solar system objects and so on) for the training of *Gaia* algorithms are being carried out by different groups.

This paper is the first of a series, which will present different aspects of the survey and of its data products. The series will include technical papers on the instrumental characterization, data papers presenting flux tables, photometric measurements and light curves of our spectrophotometric standard stars (SPSS) candidates, and scientific follow-up papers based on survey data and, when needed, on additional data.

This paper presents the ongoing observational survey aimed at building the grid of SPSS for the absolute flux calibration of *Gaia* spectra and integrated magnitudes. The structure of the paper is the following. The *Gaia* external calibration model is briefly illustrated in Section 2; the selection criteria and a list of candidate SPSS are presented in Section 3; the observing campaigns and facilities are described in Section 4; a description of the data treatment principles and methods can be found in Section 5; and a set of preliminary results is presented in Section 6.

2 FLUX CALIBRATION MODEL

Calibrating (spectro)photometry obtained from the usual type of ground-based observations (broad-band imaging, spectroscopy) is not a trivial task, but the procedures are well known (see e.g. Bessell 1999) and many groups have developed sets of appropriate standard stars for the more than 200 photometric known systems and for spectroscopic observations.

In the case of *Gaia*, several instrumental effects – much more complex than those usually encountered – redistribute light along the spectral energy distribution (SED) of the observed objects. The most difficult *Gaia* data to calibrate are the BP and RP slitless spectra, requiring a new approach to the derivation of the calibration model and to the SPSS grid needed to perform the actual calibration. Some important complicating effects are the following.

(i) The large focal plane with its large number of CCDs implies that different observations of the same star will be generally on different CCDs, with different quantum efficiencies, optical distortions, transmissivity and so on. Therefore, each wavelength as well as each position across the focal plane has its (sometimes very different) point spread function (PSF).

(ii) Time delayed integration continuous reading mode, combined with the need of compressing most of the data before on-ground transmission, make it necessary to translate the full PSF into a linear (compressed into 1D) line spread function, which of course adds complication into the picture.

[3] Tsalmantza & Bailer-Jones (2009), as many other documents cited in the following, is a *Gaia* technical report that is normally not available to the public. We nevertheless will cite some of these documents because they contain more detailed discussions of the topics treated here, or simply to give appropriate credit to work that was done previously. Future papers of this series will enter in more technical and scientific details. Subject to approval by the ESA and the *Gaia* DPAC governing bodies, *Gaia* technical reports can be provided to interested readers by the authors.

(iii) In-flight instrument monitoring is foreseen, but never comparable to the full characterization that will be performed before launch, so the real instrument – at a certain observation time – will be slightly different from the theoretical one assumed initially, and this difference will change with time.

(iv) Finally, radiation damage [or charge transfer inefficiencies (CTIs)] deserves special mention, for it is one of the most important factors in the time variation of the instrument model (Pasquier 2011; Prod'Homme 2011; Weiler, Babusiaux & Short 2011). It has particular impact on to the BP and RP dispersed images because the objects travel along the BP and RP CCD strips in a direction that is parallel to the spectral dispersion (wavelength coordinate) and therefore the net effect of radiation damage can be to alter the SED of some spectra. Several solutions are being implemented to mitigate CTI effects, but the global instrument complexity calls for a new approach to spectra flux calibrations.

A flux calibration model is currently implemented in the photometric pipeline, which splits the calibration into an *internal* and an *external* part. The internal calibration model (Jordi et al. 2007; Fabricius et al. 2009; Jordi 2011; Carrasco et al., in preparation) uses a large number of well-behaved stars (internal standards), observed by *Gaia*, to report all observations to a *reference* instrument, on the same instrumental relative flux and wavelength scales. Once each observation for each object is reported to the internal reference scales, the absolute or *external* calibration (Montegriffo & Bellazzini 2009; Ragaini et al. 2009a,b; Ragaini, Montegriffo & Cacciari, in preparation) will use an appropriate SPSS set to report the relative flux scale to an absolute flux scale in physical units, tied to the calibration of Vega (see also Section 3). Alternative approaches where the internal and external calibration steps are more interconnected are being tested to maximize the precision and the accuracy of the *Gaia* calibration (Brown et al. 2010; Montegriffo 2011; Montegriffo et al. 2011; Carrasco et al., in preparation). The *Gaia* calibration model was also described by Pancino (2010), Jordi (2011) and Cacciari (2011).

The final flux-calibrated products will be (i) averaged (on all transits – or observations) white light magnitudes, G, (ii) integrated BP/RP magnitudes, $G_{\rm BP}$ and $G_{\rm RP}$, (iii) flux-calibrated BP/RP spectra and (iv) RVS spectra and integrated $G_{\rm RVS}$ magnitudes, possibly also flux calibrated (Trager 2010). The $G_{\rm BP} - G_{\rm RP}$ colour will be used to correct for chromaticity effects in the global astrometric solution. Only for specific classes of objects, epoch spectra and magnitudes will be released, with variable stars as an obvious example.

The external calibration model contains – as discussed – a large number of parameters, requiring a large number (about 200) of calibrators. With the standard calibration techniques (Bessell 1999), the best possible calibrators are hot, almost featureless, stars such as white dwarfs (WDs) or hot subdwarfs. Unfortunately, these stars are all similar to each other, forming an intrinsically degenerate set. The *Gaia* calibration model instead requires to differentiate as much as possible the calibrators, by including smooth spectra, but also spectra with absorption features, both narrow (atomic lines) or wide (molecular bands), appearing both on the blue and the red side of the spectrum.[4] An experiment described by Pancino (2010) shows that the inclusion of just a few M stars[5] with large molecular absorptions in the *Gaia* SPSS set can improve the calibration of similarly red stars by a factor of more than 10 (from a formal error of 0.15 mag to an error smaller than 0.01 mag).

In conclusion, the complexity of the instrument reflects in a complex calibration model, which requires a large set of homogeneously calibrated SPSS, covering a range of spectral types. No such data base exists in the literature, and new observations are necessary to build it.

3 THE CANDIDATE SPSS

The *Gaia* photometric calibration model implies specific needs as it comes to (i) the selection criteria of the SPSS candidates and (ii) the characteristics of their flux tables (i.e. their calibrated spectra). The derived formal requirements (van Leeuwen, Pancino & Altavilla 2011) define both the SPSS grid and the observing needs and can be summarized as follows:

(i) spectral resolution $R = \lambda/\delta\lambda \simeq 1000$, i.e. they should oversample the *Gaia* BP/RP resolution by a factor of 4–5 at least;

(ii) wavelength coverage of 3300–10 500 Å, corresponding to the full coverage of the BP and RP spectrophotometers;

(iii) large sample (approximately 200–300 stars), covering different spectral types, although a large fraction should consist of hot stars, as featureless as possible;

(iv) magnitude range $9 < V < 15$ mag: when observed by *Gaia* they should ensure an end-of-mission signal-to-noise ratio (S/N) $\simeq$ 100 over most of the wavelength range, without saturating;

(v) typical uncertainty on the absolute flux, with respect to the assumed calibration of Vega (Bohlin & Gilliland 2004; Bohlin 2007)[6] of $\simeq$3 per cent, excluding small troubled areas in the spectral range (telluric bands residuals, extreme red and blue edges), where it can be somewhat worse;

(vi) very homogeneous data treatment and quality, i.e. the SPSS flux tables should have $\simeq$1 per cent internal precision;

(vii) photometric stability within $\pm$5 mmag, necessary to ensure the above accuracy and precision.

The CALSPEC[7] (Bohlin 2007) and the Stritzinger et al. (2005) data bases are very good starting points (see also Bessell & Murphy 2012, for further references), but new observations are needed.

It is clear that if we add the requirements derived from a ground-based campaign[8] to the above ones, it becomes very difficult to assemble the grid in a relatively short time. Therefore, we decided to proceed in steps. The link between Vega and our SPSS will be ensured by three *pillars* (Section 3.1); these will enable to calibrate the *primary SPSS* (Section 3.2), our ground-based calibrators spread over the whole sky. The primary SPSS will in turn enable to calibrate our *secondary SPSS* (Section 3.3), which constitute the actual *Gaia*

[4] Including emission-line objects in our set of calibrators is problematic. Emission-line stars are often variable and thus do not make good calibrators. For the same reasons, quasar calibrations are also problematic because they are typically faint for our ground-based campaigns. Thus, with this calibration model we do not expect to be able to calibrate with very high accuracy emission-line objects.

[5] While M giants show almost always variations of the order of 0.1–0.2 mag, and thus are not useful as flux standards, M dwarfs rarely do (Eyer & Mowlavi 2008).

[6] A great promise for the future of flux calibrations comes from the *ACCESS* mission (Kaiser et al. 2010). We tried to include a few of their primary targets in our SPSS candidates list.

[7] http://www.stsci.edu/hst/observatory/cdbs/calspec.html

[8] Observations must be feasible with 2–4 m class telescopes, all year round from both hemispheres, and the SPSS must be free from relatively bright companions that might be seen as separate objects from space, but are close enough to contaminate the SPSS aperture photometry and wide-slit spectra, owing to the Earth's atmospheric seeing.

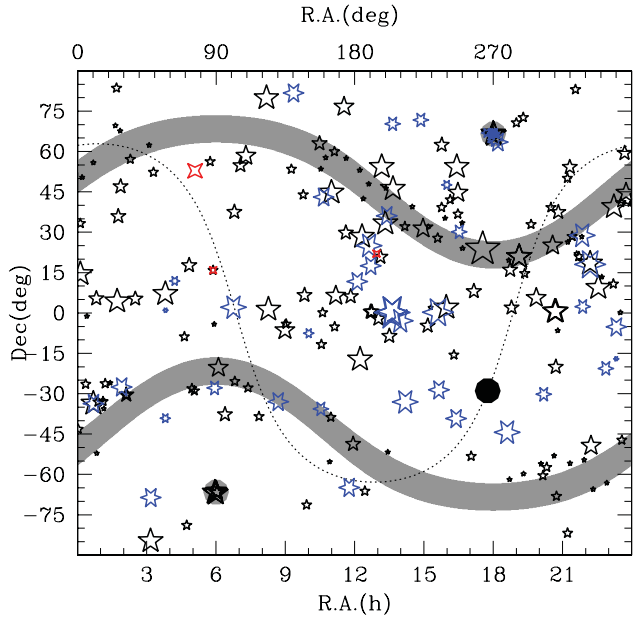

Figure 2. Distribution of our SPSS candidates on the sky. The Galactic plane and Galactic Centre are marked with a dotted line and a large black circle, respectively. The ecliptic poles are marked as two large grey circles, and two stripes at ±45° from the ecliptic poles (roughly where *Gaia* is observing more often) are shaded in grey. Our *pillars* are shown as three four-pointed stars, the *primary SPSS candidates* as six-pointed stars, and the *secondary SPSS candidates* as five-pointed stars. The stars' size is proportional to the SPSS brightness, ranging from $V \simeq 8$ (largest symbols) to 15 mag (smallest symbols), approximately.

grid, together with the eligible *primaries*. The basic principles of our calibration strategy were first outlined by Bellazzini et al. (2006). The sky distribution of our candidates is shown in Fig. 2, while the magnitude and spectral type distributions are shown in Fig. 3. More

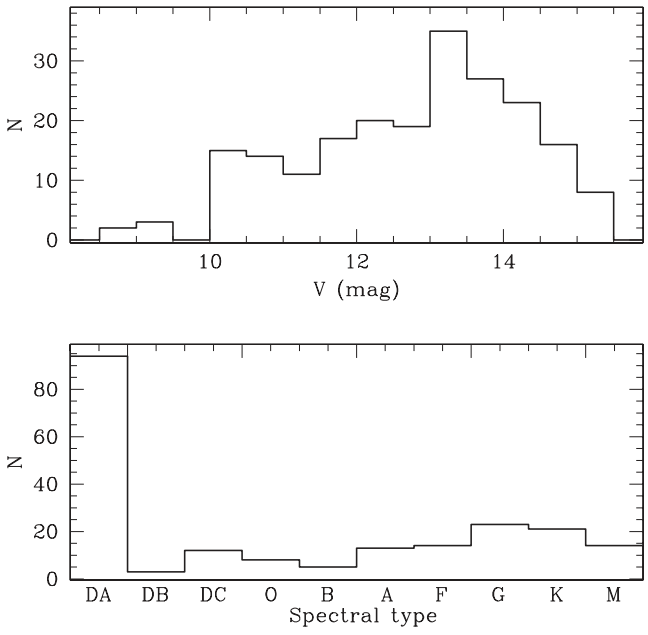

Figure 3. Distribution of all our SPSS candidates in magnitude (top panel) and spectral type (bottom panel).

Table 1. Pillars.

Star	RA (J2000)[a] (hh:mm:ss)	Dec. (J2000)[a] (dd:pp:ss)	B (mag)	V (mag)	Type[b]
G191-B2B	05:05:30.61	+52:49:51.95	11.46[c]	11.78[c]	DA0
GD 71	05:52:27.63	+15:53:13.37	12.78[b]	13.03[b]	DA1
GD 153	12:57:02.33	+22:01:52.52	13.07[b]	13.35[b]	DA1

[a] van Leeuwen (2007) coordinates; [b]Bohlin, Lindler & Riess (2005) magnitudes and spectral types; [c]Landolt & Uomoto (2007) magnitudes.

details on the selection criteria, sources and candidate lists can be found in Altavilla et al. (2008, 2010b).

3.1 Pillars

Our three pillars are the CALSPEC pillars and were selected from Bohlin, Colina & Finley (1995) and Bohlin (1996). They are the DA (pure hydrogen atmosphere) WDs named G191-B2B, GD 71 and GD 153, three well known and widely used standards. A fourth star from Bohlin et al. (1995), HZ 43, was excluded from our list because it is member of a binary system. Its companion, a dMe star (Dupuis et al. 1998), at a distance of ≃3 arcsec, is brighter longwards of ≃7000 Å (Bohlin, Dickinson & Calzetti 2001), and therefore not usable in our ground-based campaign, where the actual seeing ranges from ≃0.5 arcsec up to >2 arcsec in some cases and the slit width is 10–12 arcsec for our spectra.

The flux-calibrated spectra of the *pillars*, available in the CALSPEC data base, are tied to the revised Vega flux,[9] and their flux calibrations are based on the comparison of WD model atmospheres[10]and spectra obtained with the Faint Object Spectrograph (FOS) on-board *Hubble Space Telescope* (*HST*). The *pillars* are in the temperature range $32\,000 \leq T_{\rm eff} \leq 61\,000$ K and the FOS spectrophotometry agrees with the model fluxes to within 2 per cent over the whole UV–visible range. In addition, the simulated B and V magnitudes of the data agree to better than 1 per cent with the Landolt photometry (Landolt & Uomoto 2007).

Some of the most recent literature measurements for the three *pillars* are listed in Table 1.

3.2 Primary SPSS candidates

The candidate *primary* SPSS are 44 bright ($9 \lesssim V \lesssim 14$ mag – see also Table 2), well-known spectrophotometric standards with spectra already in the CALSPEC flux scale, or which can be easily tied to that scale with dedicated ground-based observations. We selected them according to the criteria outlined above, and with the additional criterion that the sample should be observable from both hemispheres, all year round, with 2–4 m class telescopes, as mentioned above.

We searched for candidates the best existing data sets, such as CALSPEC, Oke (1990), Hamuy et al. (1992, 1994) and Stritzinger et al. (2005). As already noted, the *primary* SPSS will be calibrated

[9] Vega was calibrated using Space Telescope Imaging Spectrograph (STIS) observations (Bohlin & Gilliland 2004) and the calibration was later revised by Bohlin (2007).

[10] Hubeny non-local thermodynamic equilibrium models (Hubeny & Lanz 1995). See also Bohlin (2007) and references therein. In particular, these model flux distributions are normalized to an absolute flux of Vega of 3.46×10^{-9} erg cm^{-2} s^{-1} Å^{-1} at 5556 Å.

using the *pillars*, and will constitute our grid of ground-based calibrators for the *secondary* SPSS. Those *primaries* which a posteriori will satisfy also the criteria outlined for the *secondary* SPSS (e.g. will have an end-of-mission satisfactory S/N when observed by *Gaia*) will be included in the final list of *Gaia* SPSS. The *primary* SPSS candidates are listed in Table 2 along with some recent literature information.

We mention here that one of the CALSPEC standards, star 1740346, was found to be a variable with an amplitude of the order of 10 mmag, and is probably a δ Scuti type variable, as described in Section 6.3. We are gathering additional data to characterize its variability.

Table 2. Primary SPSS candidates.

Star	RA (J2000) (hh:mm:ss)	Dec. (J2000) (dd:pp:ss)	B (mag)	V (mag)	Type
White dwarfs and hot subdwarfs					
EG 21	03:10:31.02[a]	−68:36:03.39[a]	11.42[b]	11.38[b]	DA3[c]
GD 50	03:48:50.20[d]	−00:58:31.20[d]	13.79[e]	14.06[e]	DA2[c]
HZ 2	04:12:43.55[f]	+11:51:49.00[f]	13.79[g]	13.88[g]	DA3[c]
LTT 3218	08:41:32.56[h]	−32:56:34.90[h]	12.07[e]	11.85[e]	DA[i]
AGK+81266	09:21:19.18[a]	+81:43:27.64[a]	11.60[g]	11.94[g]	O[j]
GD 108	10:00:47.37[k]	−07:33:30.50[k]	13.34[l]	13.58[l]	B[k]
Feige 34	10:39:36.74[a]	+43:06:09.25[a]	10.84[g]	11.18[g]	DO[j]
LTT 4364	11:45:42.92[a]	−64:50:29.46[a]	11.69[e]	11.50[e]	DQ6[i]
Feige 66	12:37:23.52[a]	+25:03:59.87[a]	10.22[g]	10.51[g]	O[j]
Feige 67	12:41:51.79[a]	+17:31:19.75[a]	11.48[g]	11.82[g]	O[j]
HZ 44	13:23:35.26[a]	+36:07:59.51[a]	11.38[g]	11.67[g]	O[j]
GRW+705824	13:38:50.47[a]	+70:17:07.62[a]	12.68[g]	12.77[g]	DA3[j]
EG 274	16:23:33.84[a]	−39:13:46.16[a]	10.89[b]	11.02[b]	DA2[c]
EG 131	19:20:34.93[a]	−07:40:00.05[a]	12.35[ee]	12.29[ee]	DBQA5
LTT 7987	20:10:56.85[a]	−30:13:06.64[a]	12.27[e]	12.21[e]	DA4[m]
G93−48	21:52:25.38[a]	+02:23:19.56[a]	12.73[e]	12.74[e]	DA3[c]
LTT 9491	23:19:35.44[n]	−17:05:28.40[n]	14.13[g]	14.11[g]	DB3[i]
Feige 110	23:19:58.40[a]	−05:09:56.21[a]	11.53[g]	11.83[g]	O[o]
Other hot stars (O, B and A)					
HD 37725	05:41:54.37[p]	+29:17:50.93[p]	8.12[gg]	8.31[gg]	A3[hh]
HILT 600	06:45:13.37[p]	+02:08:14.70[p]	10.62[b]	10.44[b]	B1[q]
Feige 56	12:06:47.23[a]	+11:40:12.64[a]	10.93[b]	11.06[b]	B5p[b]
SA 105−448	13:37:47.07[p]	−00:37:33.02[p]	9.44[r]	9.19[r]	A3[s]
HD 121968	13:58:51.17[a]	−02:54:52.32[a]	10.08[r]	10.26[r]	B1[t]
CD −32 9927	14:11:46.32[p]	−33:03:14.30[p]	10.84[u]	10.44[u]	A0[o]
LTT 6248	15 38 59.66[v]	−28 35 36.87[v]	12.29[e]	11.80[e]	A[b]
1743045	17:43:04.48[f]	+66:55:01.60[f]	13.80[w]	13.52[w]	A5[x]
1805292	18:05:29.28[f]	+64:27:52.00[f]	12.50[w]	12.06[w]	A6[w]
1812095	18:12:09.57[f]	+63:29:42.30[f]	11.90[w]	11.80[w]	A5[w]
BD +28 4211	21:51:11.02[a]	+28:51:50:36[a]	10.17[g]	10.51[g]	Op[j]
Cooler stars (F, G and K)					
CD −34 241[y]	00:41:46.92[p]	−33:39:08.51[p]	11.71[b]	11.23[b]	F[b]
LTT 1020	01:54:50.27[v]	−27:28:35.74[v]	12.06[e]	11.51[e]	G[b]
LTT 1788	03:48:22.67[n]	-39:08:37.20[n]	13.61[e]	13.15[e]	F[b]
LTT 2415	05:56:24.74[a]	−27:51:32.35[a]	12.60[e]	12.20[e]	G[i]
LTT 3864	10:32:13.60[v]	−35:37:41.80[v]	12.65[e]	12.17[e]	F[b]
SA 105−663	13:37:30.34[a]	−00:13:17.37[a]	9.10[s]	8.76[s]	F[z]
P 41-C	14:51:57.99[aa]	+71:43:17.38[aa]	12.84[bb]	12.16[bb]	G0[cc]
SA 107−544	15:36:48.10[p]	−00:15:07.11[p]	9.44[s]	9.04[s]	F3[z]
P 177-D	15:59:13.57[f]	+47:36:41.90[f]	13.96[dd]	13.36[dd]	G0[cc]
P 330-E	16:31:33.82[f]	+30:08:46.50[f]	13.52[dd]	12.92[dd]	G0[cc]
KF08T3	17:55:16.23[f]	+66:10:11.70[f]	14.30[cc]	13.50[cc]	K0[x]
KF06T1	17:57:58.49[f]	+66:52:29.40[f]	14.50[cc]	13.52[cc]	K1[x]
KF06T2	17:58:37.99[f]	+66:46:52.20[f]	15.10[cc]	13.80[cc]	K1[x]
KF01T5	18:04:03.80[x]	+66:55:43.00[x]	–	13.56[x]	K1[x]
LTT 7379	18:36:25.95[a]	−44:18:36.94[a]	10.83[e]	10.22[e]	G0[b]
BD +17 4708	22:11:31.37[a]	+18:05:34.17[a]	9.91[g]	9.46[g]	F8[cc]
LTT 9239	22:52:41.03[v]	−20:35:32.89[v]	12.67[e]	12.07[e]	F[b]

[a] Perryman et al. (1997); [b]Hamuy et al. (1992); [c]Bica, Bonatto & Giovannini (1996); [d]Hawarden et al. (2001); [e]Landolt (1992); [f]2MASS (Cutri et al. 2003); [g]Landolt & Uomoto (2007); [h]Bakos, Sahu & Németh (2002); [i]Bessell (1999); [j]Turnshek et al. (1990); [k]Østensen et al. (2010); [l]Colina & Bohlin (1994); [m]Holberg, Oswalt & Sion (2002); [n]Pokorny, Jones & Hambly (2003); [o]Stone & Baldwin (1983); [p]Hog et al. (1998); [q]Stone (1977); [r]Stritzinger et al. (2005); [s]Landolt (1983); [t]Sembach & Savage (1992); [u]Kilkenny & Menzies (1989); [v]Salim & Gould (2003); [w]Bohlin et al. (2011); [x]Reach et al. (2005); [y]this star was wrongly identified by Hamuy et al. (1992) as LTT 377; the case is discussed in detail in Section 6.1; [z]Drilling & Landolt (1979); [aa]Zacharias et al. (2009); [bb]Høg et al. (2000); [cc]Bohlin et al. (2005); [dd]Casagrande, Portinari & Flynn (2006); [ee]Koen et al. (2010); [ff]Sion et al. (2009); [gg]Hog et al. (1998), for approximate Johnson magnitudes the formulae $V = \mathrm{VT} - 0.090(\mathrm{BT} - \mathrm{VT})$ and $B - V = 0.850(\mathrm{BT} - \mathrm{VT})$ where used; [hh]Henry Draper Catalogue (Cannon & Pickering 1993).

3.3 Secondary SPSS candidates

The *secondary* SPSS are selected according to the criteria given above; in particular, they need to provide BP/RP spectra with an adequate end-of-mission S/N (see above). This was statistically verified for all our SPSS candidates (Carrasco et al. 2006, 2007) with a set of simulations of the expected number of transits depending on the position on the sky and on the launch conditions. Stars fainter than $V \simeq 13$ mag need to have a higher number of transits to gather sufficient end-of-mission S/N when observed by *Gaia*. The candidates surviving this test are presented in Table 4 along with some recent literature information. Not all literature data (especially magnitudes and spectral types) have the same precision,[11] but we gathered the best data available, to our knowledge; we will hopefully produce more precise information from our own data and, later, from *Gaia*. Our source catalogues were mainly (but not only) the following.

(i) The '*Catalog of Spectroscopically Identified White Dwarfs*' (McCook & Sion 1999), containing 2249 stars in the original paper and 12 876 in the online – regularly updated – catalogue[12] at the time of writing.

(ii) '*A Catalog of Spectroscopically Confirmed White Dwarfs from the Sloan Digital Sky Survey Data Release 4 (SDSS)*' (Eisenstein et al. 2006), containing 9316 objects. The complete data set is available online.[13]

[11] Literature data come from a variety of heterogeneous sources, and are determined with many different methods. In particular, in Tables 2 and 4, the most uncertain magnitudes are those derived with the approximated formulae from the Tycho magnitudes (Hog et al. 1998), while the most uncertain spectral types are the ones roughly estimated by us from the Carney et al. (1994) temperatures.

[12] http://www.astronomy.villanova.edu/WDCatalog/index.html

[13] http://iopscience.iop.org/0067-0049/167/1/40/datafile1.txt

(iii) A list of 121 DA WDs for which there are *FUSE*[14] data (Barstow, private communication).

(iv) A selection of metal-poor stars from '*A survey of proper motion stars. 12: an expanded sample*' (Carney et al. 1994) containing 52 stars (Korn, private communication).

(v) '*The HST/STIS Next Generation Spectral Library*' (NGSL; Gregg et al. 2004)[15] containing 378 bright stars covering a wide range in abundance, effective temperature and luminosity.

(vi) The catalogues from '*The M dwarf planet search programme at the ESO VLT + UVES. A search for terrestrial planets in the habitable zone of M dwarfs*' (Zechmeister, Kürster & Endl 2009) and from '*Rotational Velocities for M Dwarfs*' (Jenkins et al. 2009), particularly useful for the selection of red stars.

(vii) The '*Medium-resolution Isaac Newton Telescope Library of Empirical Spectra (MILES)*'[16] (Sánchez-Blázquez et al. 2006) data base containing 985 spectra obtained at the 2.5-m Isaac Newton Telescope covering the range 3525–7500 Å.

(viii) *'Sloan Extension for Galactic Understanding and Exploration (SEGUE): A Spectroscopic Survey of 240 000 Stars with $g = 14$–20'* (Yanny et al. 2009), containing $\simeq$240 000 moderate-resolution spectra from 3900 to 9000 Å of fainter Milky Way stars ($14.0 \leq g \leq 20.3$) of a wide variety of spectral types and classes. In particular, we made use of the re-analysis by Tsalmantza & Bailer-Jones (2009) and Tsalmantza et al. (2012) to select a few suitably bright stars.

(ix) *'The Ecliptic Poles Catalogue Version 1.1'* (Altman & Bastian 2009), a preliminary version of the photometric catalogue that will be used by *Gaia* in the initial observation phases, containing 150 000 stars down to $V \simeq 22$ mag, in a region of approximately 1 deg^2 around the Northern and Southern ecliptic poles.

(x) The WD online catalogue maintained by A. Kawka,[17] and information from Kawka et al. (2007).

(xi) A provisional list of targets for the *ACCESS* mission (Kaiser et al. 2007, 2010), provided by M. E. Kaiser (private communication).

Other references can be found in Table 4. All the lists were merged and cross-checked to eliminate redundant entries. The clean list ($\simeq$13 500 stars) was then used to extract a subsample ($\simeq$300 stars) according to the criteria outlined above.

During the course of the survey, we rejected a few of the original $\simeq$300 candidates because they were found to be binaries, variables or they showed close companions on the basis of our literature monitoring and/or of our data. The rejection procedure, along with a few interesting cases, is described in Section 6. A few more candidates may be rejected during the course of the campaign, and some candidates might be added if needed by the *Gaia* photometric pipeline, once it is run on real data.

4 THE SURVEY

Our survey is split into two campaigns – the *main campaign* dedicated to obtaining spectrophotometry of all our candidate SPSS and the *auxiliary campaign* dedicated to monitoring the constancy of our SPSS on relevant time-scales.

4.1 Main campaign

Classical spectrophotometry (Bessell 1999) would clearly be the best approach to obtain absolutely calibrated flux spectra if we had a dedicated telescope. However, a pure spectrophotometric approach would require too much time, given that we need high S/N of 300 stars, in photometric sky conditions, which are rare except maybe in a few sites. We thus decided for a combined approach (Bellazzini et al. 2006), in which spectra are obtained even if the sky is non-photometric,[18] providing the correct spectral shape of our SPSS (what we will call '*relative flux calibration*'). Then, imaging in photometric conditions and in three bands (generally *B*, *V* and *R*, but sometimes also *I* and, more rarely, *U*) is obtained and calibrated magnitudes are used to scale the spectra to the correct zero-point ('*absolute flux calibration by comparison*').

The calibrated magnitudes of SPSS will be obtained through *at least* three independent observations in photometric conditions. Our sample contains some photometric standards from Landolt (1992) and Landolt & Uomoto (2007), and a few secondary Stetson standards[19] (see Stetson 2000, and online updates). By comparing the obtained magnitudes and synthetic magnitudes derived from the relatively calibrated spectra, we can obtain the necessary zero-point corrections to correct our spectral flux calibration. To those spectra obtained in photometric conditions (at the moment approximately 20–25 per cent of the total) we will apply the classical method, and this control sample will allow us to check the validity of the combined spectroscopy plus photometry approach.

4.2 Constancy monitoring

This kind of monitoring is necessary for a few reasons. Even stars used for years as spectrophotometric standards were found to vary when dedicated studies have been performed (see e.g. G24−9, which was found to be an eclipsing binary by Landolt & Uomoto 2007), and even stars that are apparently safe may show unexpected variations. Our own survey has already found a few variables and suspected variables, including one of the CALSPEC standards (Section 6.3).

WDs may show variability with (multi)periods from about 1 to 20 min and amplitudes from about 1–2 up to 30 per cent, i.e. ZZ Ceti type variability. We have tried to exclude stars within the instability strips for DAV (Castanheira et al. 2007), DBV and DOV but in many cases the existing information was not sufficient (or sufficiently accurate) to firmly establish the constant nature of a given WD. Hence, many of our candidate SPSS needed to be monitored for constancy on *short time-scales*, of the order of 1–2 h. Similar considerations are valid for hot subdwarfs (Kilkenny 2007).

Also redder stars are often found to be variable: for example, K stars have shown variability of 5–10 per cent with periods of the order of days to tens of days (Eyer & Grenon 1997). In addition, binary systems are frequent and eclipsing binaries can be found at all spectral types. Their periods can span a range from a few hours to hundreds of days, most of them having $P \simeq 1$–10 d (Dvorak 2004). Thus, in addition to our short-term monitoring, we are observing all our SPSS on *longer time-scales*, of about 3 yr, with a random

[14] http://fuse.pha.jhu.edu/
[15] http://archive.stsci.edu/prepds/stisngsl/
[16] http://www.ucm.es/info/Astrof/miles/miles.html
[17] http://sunstel.asu.cas.cz/~kawka/Mainbase.html

[18] The cloud coverage must produce grey extinction variations, i.e. the extinction must not alter significantly the spectral shape. This condition is almost always verified in the case of veils or thin clouds (Oke 1990; Pakštiene & Solheim 2003), and can be checked a posteriori for each observing night.
[19] http://www4.cadc-ccda.hia-iha.nrc-cnrc.gc.ca/community/STETSON/

phase sampling approximately four times a year, which should be enough to detect variability, although not for a proper characterization of these newly discovered variables. Unlike the short-term monitoring, the long-term monitoring can be picked up by *Gaia* once it starts operations. *Gaia* data will help in the characterization and parametrization of the detected variables by providing, on average, ≃80 sets of spectra and integrated magnitudes in its 5 years of operation.

We use relative photometry measurements, with respect to field stars, for both our short-term (1–2 h) and long-term (3 yr) monitoring campaigns, aiming at excluding all stars with a variability larger than ±5 mmag, approximately. Obviously, as soon as a target is recognized as variable, it is excluded from our candidate list, but we are aware that some characterization of the variability is of scientific value, so whenever possible we follow-up our new variable stars with imaging, more detailed light curves and, when necessary, spectroscopy.

4.3 Observing facilities and status

We have considered a long list of available facilities in both hemispheres (Federici et al. 2006; Altavilla et al. 2010a). The eligible instruments must be capable of obtaining low-resolution spectroscopy – with the characteristics described in Section 3 – and Johnson–Cousins photometry. At least one site in the North and one in the South with a high probability of having photometric sky conditions were necessary. We eventually selected six facilities:

(i) EFOSC2@NTT at the European Southern Observatory (ESO) La Silla Observatory, Chile, our Southern facility for spectroscopy and absolute photometry, and for some constancy monitoring;
(ii) ROSS@REM at the ESO La Silla Observatory, Chile, our Southern facility for relative photometry;
(iii) CAFOS@2.2 m at the Calar Alto Observatory, Spain, one of our Northern spectrographs and imagers, for absolute and relative (spectro)photometry;
(iv) DOLoRES@TNG at the Roque de Los Muchachos in La Palma, Spain, one of our Northern spectrographs and imagers, for absolute and relative (spectro)photometry;
(v) LaRuca@1.5 m at the San Pedro Mártir Observatory, Mexico, our Northern source of absolute and relative photometry;
(vi) BFOSC@Cassini in Loiano, Italy, providing a few spectra and more relative photometry in the Northern hemisphere.

Given the diversity of instruments and observing conditions, we enforced a set of strict observing protocols (Pancino et al. 2008, 2009, 2011), concerning all aspects of the photometry and spectroscopy observations, including requirements about the calibration strategy, and on-the-fly quality control (QC) of data acquired at the telescope (see also Sections 4.1 and 4.2). Observations started in 2007. At the time of writing, the survey has been awarded more than 400 nights of observing time, both in visitor and service mode, of which 25–35 per cent was lost due to bad weather or technical reasons, or was of non-optimal quality. The main campaign should be completed within 2012, with the last ESO run assigned in 2012 July and the last Calar Alto run in 2012 May. The short-term variability monitoring is 85 per cent complete and the long-term monitoring will take more time and will probably be completed around 2013–2014.

5 DATA TREATMENT AND DATA PRODUCTS

The required precision and accuracy of the SPSS calibration imposes the adoption of strict protocols of instrument characterization, data reduction, QC and data analysis. We will briefly outline below our data treatment methods, while more details will be published in future papers of the series, presenting our data products. At the time of writing, reductions are ongoing: pre-reduction of the obtained data is more than 50 per cent complete, while the analysis is advancing for short-term (1–2 h) constancy monitoring (≃35 per cent complete) and less complete for spectroscopy (≃20 per cent) and absolute photometry (just started). Long-term (3 yr) constancy monitoring observations are still incomplete.

5.1 Familiarization plans

We obtained our data from a variety of instruments, which also were upgraded or modified during the course of the observations, for example a few CCDs were substituted by new and better CCDs. A strict characterization of the used instruments was needed, requiring additional calibration data, taken during daytime, twilight and also nighttime. We called these technical projects 'familiarization plans' (Altavilla et al. 2011; Marinoni et al., in preparation). Their results will be published in subsequent technical papers of this series, and they can be roughly summarized as follows:

(i) CCD familiarization plan, containing a study of the dark and bias frames' stability; the shutter characterization (shutter times and delays); and the study of the linearity of all employed CCDs;
(ii) instrument familiarization plan studying the stability of imaging and spectroscopy flats, the study of fringing and the lamp flexures of the employed spectrographs;
(iii) site familiarization plan (in preparation), providing extinction curves, extinction coefficients, colour terms and a study of the effect of 'calima'[20] on the spectral shape.

As a results of these studies, specific recommendations for observations and data treatment were defined.

5.2 Pre-reductions

Data reductions were performed mostly with IRAF[21] and IRAF-based pipelines. The detailed data reduction protocols are described in *Gaia* technical reports (Marinoni et al. 2012; Altavilla et al., in preparation; Cocozza et al., in preparation; Marinoni et al., in preparation).

For imaging, we pre-reduced the frames with standard techniques, and then performed aperture photometry with SExtractor (Bertin & Arnouts 1996). SExtractor also provides many useful parameters that we will use for a semi-automated QC of each reduced frame, allowing us to identify saturated or too faint SPSS, or frames that do not contain enough good reference stars in the field to perform relative photometry. Reduced frames that pass QC and their respective photometric catalogues are stored in our local archive.

Spectroscopic reductions are less automated, relying mostly on the standard IRAF long-slit package and tasks. Spectra are pre-reduced, extracted and wavelength calibrated. Spectrophotometry

[20] Calima is a dust wind originating in the Sahara air layer, which often affects observations in the Canary Islands.
[21] IRAF is the Image Reduction and Analysis Facility, a general purpose software system for the reduction and analysis of astronomical data. IRAF is written and supported by the IRAF programming group at the National Optical Astronomy Observatories (NOAO) in Tucson, Arizona. NOAO is operated by the Association of Universities for Research in Astronomy (AURA), Inc., under cooperative agreement with the National Science Foundation.

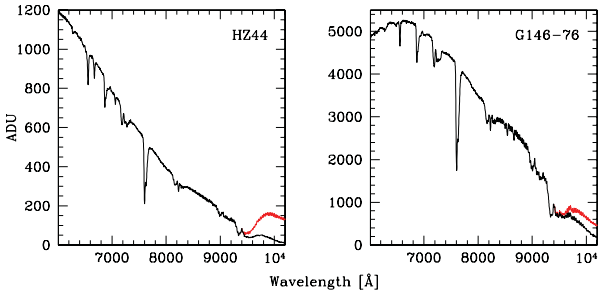

Figure 4. Second-order contamination on DOLoRes@TNG spectra of a blue star (left-hand panel) and a red star (right-hand panel); the black lines are the corrected spectra, while the red lines above, starting at about 9500 Å, show the contaminated spectra.

is obtained with a wide slit (five to six times the seeing, at least; generally the widest available slits are 10 or 12 arcsec). Narrow-slit spectra are also observed (typically with a slit of 1–2.5 arcsec, depending on the instrument), to obtain a better wavelength calibration. In some cases (slit larger than 1.5 times the seeing), we will attempt to correct the narrow-slit spectra for differential light losses; tests show that this can be done in most cases with a third-order polynomial fit. The corrected narrow-slit spectra will thus add to the S/N of wide-slit spectra, and will also help in beating down the fringing, because the fringing patterns of wide- and narrow-slit spectra are different.[22] Extracted and wavelength-calibrated 1D spectra are stored locally for future processing, if they pass some basic QC (not saturated or too faint, no close companions in the slit and so on).

5.3 Higher level spectra treatment

After spectra are extracted and wavelength calibrated, they are corrected for telluric absorption features and for second-order contamination (see below). The blue and red spectral ranges, which are observed separately with the available instruments, are joined after performing a relative calibration using the available *pillar* or *primary* observations taken on the same night at different airmasses.

To illustrate the quality of the reduction procedures, we show in Fig. 4 our second-order contamination correction for a blue and a red star. The effect arises when light from blue wavelengths, from the second dispersed order of a particular grism or grating, falls on the red wavelengths of the first dispersed order. Such contamination usually happens when the instrument has no cross-disperser. Of the instruments we use (Section 4.3), only EFOSC2@NTT and DOLoRes@TNG present significant contamination. To map the blue light falling on to our red spectra, we adapted a method proposed by Sánchez-Blázquez et al. (2006) and applied it to dedicated observations (Altavilla et al., in preparation). Our wavelength maps generally allow us to recover the correct spectral shape to within a few per cent, as tested on a few CALSPEC standards observed with both TNG and NTT.

If the spectra were observed in photometric conditions, after the above manipulations the flux calibration is complete and ready to be checked. Otherwise, the shape of the spectrum is recovered, but an additional zero-point correction is required. Different levels of intermediate data products are stored after basic QC, including spectra with and without telluric correction or second-order contamination correction.

5.4 Absolute and relative photometry

Photometry observations are taken in the form of a night point (absolute or relative, depending on sky conditions) or a time series. The night point is a triplet of images in each of three filters (*B*, *V*, *R*, and sometimes also *I* or *U*) taken consecutively. A series lasts at least one hour, contains at least 30 exposures and is taken with the bluest available filter (*B* in most cases, except for REM, where we use *V*). The SExtractor catalogues are cross-matched with CataXcorr[23] to identify the SPSS and the reliable reference stars in the surrounding field.

Absolute photometry is then performed in a standard way, using observations of two or three standard fields (Landolt 1992) at different airmasses during the night. Observations of the same SPSS are taken repeatedly at different times and, when possible, different sites, to be able to identify any hidden systematics. Some stars in our candidates list are spectrophotometric standards (Landolt 1992; Stetson 2000; Landolt & Uomoto 2007) that will be used to check the quality of our measurements. The final calibrated magnitudes will be used to correct the zero-point of spectra observed in non-photometric (but grey absorption) sky conditions, as explained later.

Relative photometry is performed using the difference between the SPSS and the available field stars' magnitudes (at least two field stars are required). Reference stars must be non-saturated, not too faint, present in all frames and non-variable. Some preliminary results of this procedure are discussed in Section 6. The target precision of at least 10 mmag, necessary to meet our calibration requirements (Section 3), is generally always reached with BFOSC, EFOSC2, LaRuca, DOLoRes and CAFOS, and most of the times also with ROSS@REM, the robotic telescope in La Silla.

The final data products of the photometry procedure are absolute magnitudes and differential light curves (on 1–2 h and 3 yr timescales) with their respective uncertainties.

5.5 Final flux tables

All the relatively (if the night was non-photometric but grey) and absolutely (if the night was photometric) calibrated spectra will now have the correct spectral shape. The absolutely calibrated spectra obtained in different nights or with different telescopes for each star will be compared to study hidden systematics (if any). Some of our targets belong to widely used spectrophotometric data sets (see Section 3), and will be our anchor point to check our flux scale and to find potential problems.

The relatively calibrated spectra will need a zero-point correction. We will thus use the version including telluric absorption features to derive synthetic *B*, *V* and *R* (and, if available, *I* and *U*) magnitudes, and compare them with our calibrated magnitudes (see the previous section) to apply the necessary correction. Once this procedure

[22] The fringing pattern in the extracted spectra is a combined 1D result of a 2D pattern, in an aperture that covers a different CCD region in the wide-slit and in the narrow-slit spectra. Thus, the 1D fringing pattern of these two kinds of spectra will be different.

[23] CataXcorr is part of a package dedicated to catalogue cross-matching and astrometry, developed by P. Montegriffo at the Bologna Observatory (INAF).

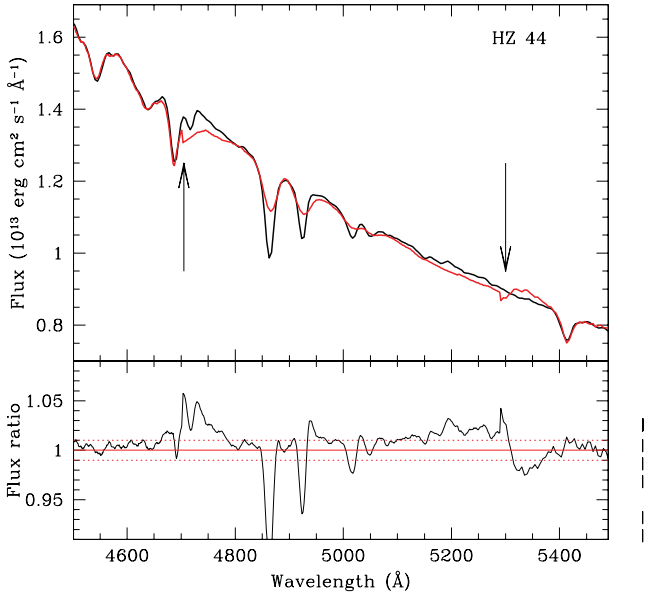

Figure 5. Top panel: comparison of our preliminary spectrum of HZ 44 (thick black line) with the CALSPEC tabulated spectrum (thick red line) in a region where we found a discrepancy (marked by the two arrows), where small ≃0.5–1.0 per cent jumps in the CALSPEC spectrum are probably due to a mismatch of two different spectra. Bottom panel: ratio between our spectrum and the CALSPEC spectrum; perfect agreement (red line) and ±1 per cent agreement (dotted red lines, our requirement) are marked.

will be completed, all the spectra obtained for each SPSS will be combined in one single spectrum: our final product. It will be necessary in many cases to use synthetic spectra to calibrate the noisy edges, or the reddest wavelength ranges, if they will not be properly cleaned from reddening.

As an example of the data quality, we show in Fig. 5 a test performed to refine our reduction procedures, where a portion of the spectrum of HZ 44 observed in a photometric night is compared with the CALSPEC flux table. We point out that this preliminary reduction did not include the proper extinction curve, but a tabulated curve from Sánchez et al. (2007); the telluric absorption features were not removed (we will use procedures similar to that by Bessell 1999); the red wavelengths are affected by fringing that we will beat down by combining observations from different telescopes whenever possible; and the extremes of the wavelength range are affected by poor S/N, so that we will have to use synthetic spectra to calibrate those extremes. Even with these limitations, we were able to meet the requirements (Section 3), because the residuals between our spectrum and the CALSPEC tabulated one were on average lower than 1 per cent, with the exception of the low-S/N red edge and the telluric absorption bands. However, some unsatisfactory jumps appeared in the comparison, between 4000 and 6000 Å, where our spectra have the highest S/N. As shown in Fig. 5 (top panel) and already noted by Bohlin et al. (2001), the jumps were due to a (minor) problem in the CALSPEC spectrum, probably where two pieces of the spectrum were joined.

Thus, we were able to identify a defect in the CALSPEC spectrum of the order of 1–2 per cent, approximately, meeting the requirements (Section 3). Similar results were obtained on test reductions of other SPSS (observed with TNG, NTT and CAHA): GD71, GD153 and G191-B2B, our *pillars*, which have the best literature data available.

To produce our final flux tables, we will need to adjust model spectra[24] to our observed spectra (as done by e.g. Bohlin 2007). This technique has proven useful to identify and fix minor problems on the spectra, and we will use it to correct for residuals from the joining of different spectral pieces, sky subtraction, telluric features correction, fringing and imperfections at the spectral extremities, where the S/N is generally lower. Also, the use of models will allow us to characterize our targets, thus providing spectral types, effective temperatures, gravities, metallicities and reddening.

6 PRELIMINARY RESULTS

We discuss in the following sections some preliminary results of our survey: a few interesting cases of problematic candidates are described, and a list of notable rejected SPSS candidates can be found in Table 3; two stars showed variability larger than ±5 mmag in our short-term constancy monitoring.

6.1 Identification and literature problems

Identification problems are common, especially when large data bases are automatically matched (as done within SIMBAD, for example) and when stars have large proper motions.

We found our first case when a discrepancy became evident between the LTT 377[25] literature spectrum (Hamuy et al. 1992, 1994) and our observed spectrum, which was more consistent with an F type rather than the expected K spectral type. We contacted the SIMBAD and ESO staff, because their sites reported the information from Hamuy et al. (1994) as well, and we concluded that the ESO standard was not LTT 377, but another star named CD −34 241, of spectral type F. This was confirmed by older literature papers such as Luyten (1957), where LTT 377 was identified as CD −34 239, and by literature proper motions and coordinates. We could trace back the error to Stone & Baldwin (1983), where the wrong association was probably done for the first time, and then propagated down to SIMBAD and ESO. The correct identification of both stars is shown in Fig. 6 (left-hand panel).[26] We decided to keep both stars in our candidates lists (see Tables 2 and 4).

A similar case was WD 0204−306 for which we obtained an unexpectedly red spectrum. We traced literature identifications back to Reid (1996), who correctly identified WD 0204−306 as associated with LP 885−23 (an M star) in a binary system, with a separation of 73 arcsec. At some point, the two stars got confused and in SIMBAD WD 0204−306 (a WD) was cross-identified with LP 885−23 (an M star). Given the reported distance between the two stars, we identified WD 0204−306 as LP 885−22, as shown in Fig. 6. Also in this case, having observations of both stars, we kept both in our *secondary SPSS candidates*. The mistake was reported to the SIMBAD staff and now the data base is corrected.

[24] We will make use of both atmosphere models from, e.g., the MARCS, Kurucz, TLUSTY and Tübingen sets (Castelli & Kurucz 2003; Lanz & Hubeny 2003, 2007; Rauch & Deetjen 2003; Gustafsson et al. 2008) or spectral libraries (e.g. Sordo & Munari 2006; Ringat 2012).

[25] At the moment of writing, the SIMBAD data base has been updated and now the correct identification is reported.

[26] The black and white finding charts in Figs 6 and 7 were created with the ESO SkyCat tool and images from the Digitized Sky Survey. SkyCat was developed by ESO's Data Management and Very Large Telescope (VLT) Project divisions with contributions from the Canadian Astronomical Data Center (CADC).

Table 3. Notable rejected SPSS candidates.

Star	RA (J2000) (hh:mm:ss)	Dec. (J2000) (dd:pp:ss)	*B* (mag)	*V* (mag)	Type	Reason for rejection
WD 0406+592	04:10:51.70[a]	+59:25:05.00[a]	14.30[a]	14.40[a]	DA[a]	Two close visual companions detected
G192−41	06:44:26.34[b]	+50:33:55.90[b]	13.91[c]	13.16[c]	G[d]	Suspected variable
WD 1148−230	11:50:38.80[a]	−23:20:34.00[a]	11.49[a]	11.76[a]	DA[a]	Two sets of coordinates and magnitudes in literature (see text)
1740346	17:40:34.68[b]	+65:27:14.80[b]	12.68[e]	12.48[e]	A5[e]	Variable, probably of δ Scuti type (CALSPEC standard)
WD 1911+135	19:13:38.68[b]	+13:36:27.70[b]	14.12[a]	14.00[a]	DA3[a]	Crowded field
WD 1943+163	19:45:31.77[b]	+16:27:39.60[b]	13.96[a]	13.99[a]	DA2[a]	Crowded field
WD 2046+396	20:48:08.18[f]	+39:51:37.33[f]	14.10[a]	14.43[a]	DA1[a]	Crowded field
WD 2058+181	21:01:16.49[b]	+18 20 55.30[b]	15.01[a]	15.00[a]	DA4[a]	One close visual companion detected
WD 2256+313	22:58:39.44[b]	+31:34:48.90[b]	14.90[g]	13.96[a]	–	Fainter than expected (see text; Oswalt, Hintzen & Luyten 1988)

[a] McCook & Sion (1999); [b] from 2MASS (Cutri et al. 2003); [c] Kharchenko (2001); [d] approximate spectral type from $T_{\rm eff}$ by Carney et al. (1994); [e] Bohlin & Cohen (2008); [f] UCAC3 (Zacharias et al. 2009); [g] USNO-B catalogue (Monet et al. 2003).

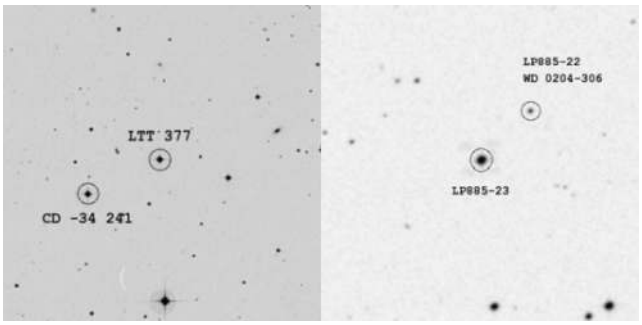

Figure 6. Correct identifications of two candidate SPSS that were wrongly identified in the literature. Left-hand panel: the case of LTT 377, which was confused with CD −34 241; the image is 15 arcmin wide, north is up and east is left. Right-hand panel: the case of WD 0204−306, which was associated with LP 885−23 instead of LP 885−22; the image is 7 arcmin wide, north is up and east on the left.

A more critical example was WD 1148−230 (Fig. 7), having very different coordinates in the McCook & Sion (1999) catalogue [coming from Stys et al. (2000) and reporting RA = $11^{\rm h}50^{\rm m}38\overset{\rm s}{.}8$ and Dec. = $-23^\circ20'34''$] and in SIMBAD. The SIMBAD coordinates were from the Two-Micron All Sky Survey (2MASS) catalogue (Cutri et al. 2003, reporting RA = $11^{\rm h}50^{\rm m}06\overset{\rm s}{.}09$ and Dec. = $-23^\circ16'14\overset{''}{.}0$). Magnitudes were also significantly different. Unlike in the previous cases, we had insufficient literature information to confirm one or the other identification, so we decided to reject this SPSS candidate, although we suspect that the mistake resides in the SIMBAD automatic association between WD 1148−230 by Stys et al. (2000) and the 2MASS catalogue.

Finally, we report on the case of WD 2256+313, which was reported to have $V = 13.96$ mag (Silvestri, Oswalt & Hawley 2002; Monet et al. 2003), but when observed in San Pedro Mártir appeared to be much fainter than that (and of uncertain spectral type; see also Oswalt et al. 1988), possibly with $V > 15$ mag, so was removed from our candidates list.

6.2 Crowded fields and visual companions

In a few cases, candidates that appeared relatively isolated on the available finding charts turned out to be in a crowded area where no aperture photometry or reliable wide-slit spectroscopy could be performed from the ground, or showed previously unseen companions. Generally, stars with high proper motion could appear isolated in some past finding chart, but later moved too close to another star to be safely observed from the ground.

One example of candidate which appeared relatively isolated judging from the McCook & Sion (1999) finding charts, but turned out to be in a crowded field when observed at San Pedro Mártir was WD 1911+135, which was promptly rejected, together with WD 1943+163 and WD 2046+396. Examples of candidates showing the presence of previously unknown and relatively bright companions were WD 0406+592 and WD 2058+181 (Fig. 8). These stars do not have a particularly high proper motion, and appeared easy to identify on the corresponding finding charts, so we did not expect them to show close visual companions, when observed from the TNG and San Pedro Mártir, respectively. Both stars were rejected.

6.3 Variability

Our auxiliary campaign started giving results as far as the short-term constancy monitoring (1–2 h) is concerned. The ability of one light curve to detect magnitude variations is measured using the spread of reference star's magnitude differences. These appear as 1σ, 2σ and 3σ limits in Fig. 9, where we present the differential light curves of our only *confirmed* variable star.

Star 1740346, one of the currently used CALSPEC standards and one of our *primary SPSS* candidates, showed variability with an amplitude of 10 ± 0.8 mmag in *B* band when observed with BFOSC@Cassini in Loiano on 2010 September 1, with DOLoRes@TNG on 2009 September 31 and with BFOSC@Cassini on 2009 May 26. The variability period is 50 min, approximately, thus showing properties typical of δ Scuti variables. A preliminary determination of 1740346 parameters can be found in Marinoni (2011), using literature data and stellar models, resulting in a mass of $\simeq 1.3\,{\rm M}_\odot$, an effective temperature of $\simeq$8300 K and a distance of $\simeq$750 pc. These parameters are also compatible with a δ Scuti type star. We are gathering detailed follow-up observations, and a complete characterization of star 1740346 will be the subject of a forthcoming paper (Marinoni et al., in preparation). The differential light curve is presented in Fig. 9 (top panel).

7 SUMMARY AND CONCLUSIONS

We have described a large (more than 400 nights) ground-based survey which started in 2007 and is expected to end in 2013–2014, aimed at building a grid of SPSS for the flux calibration of *Gaia* spectra and magnitudes. The technical complexity of *Gaia* requires a large ($\simeq$200) set of SPSS flux tables, calibrated in flux with high precision ($\simeq$1 per cent) and accuracy ($\simeq$3 per cent with respect

to Vega), and covering a range of spectral types. SPSS candidates need to be monitored for constancy (within ±5 mmag) to ensure the quoted precision in the final calibration.

We discussed the adopted calibration strategy, the selection requirements and a list of candidate SPSS. A brief overview of the adopted data reduction and analysis procedures was also presented, and more details will be discussed in a series of future papers dealing with all technical aspects, data products, photometric catalogues, flux tables and light curves. Some preliminary results were presented, showing the data quality, a few problematic cases of candidate SPSS that were rejected because of identification problems, close companions and variability. In particular, we detected a new variable star, a CALSPEC standard which is most probably a δ Scuti variable; follow-up observations for its characterization are ongoing.

All data products will be eventually made public together with each *Gaia* data release, within the framework of the DPAC publication policies. At the moment, the accumulated data and

Table 4. Secondary SPSS candidates.

Star	RA (J2000) (hh:mm:ss)	Dec. (J2000) (dd:pp:ss)	B (mag)	V (mag)	Type	Star	RA (J2000) (hh:mm:ss)	Dec. (J2000) (dd:pp:ss)	B (mag)	V (mag)	Type
WD 2359−434	00:02:10.77[1]	−43:09:56.02[1]	13.12[2]	13.05[2]	DA5[2]	HD 271759	06:00:41.34[14]	−66:03:14.03[14]	11.00[9]	11.20[9]	A2[22]
WD 0004+330	00:07:32.26[1]	+33:17:27.60[1]	13.57[2]	13.85[2]	DA1[2]	HD 271783	06:02:11.36[9]	−66:34:59.13[9]	12.63[9]	12.23[9]	F5[22]
SDSS 03932	00:07:52.22[3]	+14:30:24.72[3]	15.37[4]	15.07[4]	A0[5]	HIP 28618	06:02:27.88[6]	−66:47:28.68[6]	12.20[9]	12.30[9]	B8[22]
WD 0009+501	00:12:14.80[1]	+50:25:21.40[1]	14.78[2]	14.36[2]	DA8[2]	WD 0604−203	06:06:13.39[1]	−20:21:07.20[1]	11.75[23]	11.80[23]	DA[23]
WD 0018−267	00:21:30.73[1]	−26:26:11.46[1]	–	13.80[2]	DA9[2]	WD 0621−376	06:23:12.63[1]	−37:41:28.01[1]	11.76[2]	12.09[2]	DA1[2]
SDSS 03532	00:24:38.62[3]	−01:11:39.75[3]	15.14[4]	15.04[4]	A0[5]	WD 0644+375	06:47:37.99[6]	+37:30:57.07[6]	11.99[2]	12.08[2]	DA2[2]
WD 0038+555	00:41:21.99[1]	+55:50:08.40[1]	14.10[2]	14.08[2]	DQ5[2]	WD 0646−253	06:48:56.09[1]	−25:23:47.00[1]	13.30[2]	13.40[2]	DA2[2]
LTT 377	00:41:30.47[6]	−33:37:32.03[6]	11.97[7]	10.53[7]	K9[8]	G193−26	07:03:26.29[1]	+54:52:06.00[1]	13.59[24]	13.02[24]	G[20]
WD 0046+051	00:49:09.90[6]	+05:23:19.01[6]	12.93[2]	12.39[2]	DZ7[2]	WD 0713+584	07:17:36.26[6]	+58:24:20.51[6]	12.06[9]	12.02[9]	DA4[2]
WD 0047−524	00:50:03.68[1]	−52:08:15.60[1]	14.19[2]	14.20[2]	DA2[2]	WD 0721−276	07:23:20.10[1]	−27:47:21.60[1]	13.50[2]	13.40[2]	DA1[2]
WD 0050−332	00:53:17.44[1]	−32:59:56.60[1]	13.11[2]	13.36[2]	DA1[2]	WD 0749−383	07:51:32.58[25]	−38:28:36.41[25]	13.53[2]	13.66[2]	DA[2]
WD 0104−331	01:06:46.86[1]	−32:53:12.45[1]	13.28[2]	13.57[2]	DAZ3[2]	G251−54	08:11:06.24[6]	+79:54:29.57[6]	10.58[26]	10.01[26]	G0[26]
WD 0106−358	01:08:20.80[2]	−35:34:43.00[2]	14.54[2]	14.72[2]	DA2[2]	GJ2066	08:16:07.98[6]	+01:18:09.26[6]	11.63[7]	10.09[7]	M2[12]
WD 0109−264	01:12:11.65[9]	−26:13:27.69[9]	12.91[2]	13.15[2]	DA1[2]	G114−25	08:59:03.37[6]	−06:23:46.19[6]	12.52[27]	11.97[27]	F7[28]
WD 0123−262	01:25:24.45[1]	−26:00:43.90[1]	15.35[2]	14.95[2]	DC[2]	WD 0859−039	09:02:17.30[1]	−04:06:55.45[1]	13.02[2]	13.19[2]	DA2[2]
G245−31	01:38:39.39[1]	+69:38:01.50[1]	15.26[10]	14.50[10]	K[11]	WD 0912+536	09:15:56.23[1]	+53:25:24.90[1]	14.19[2]	13.85[2]	DB/DC[2]
WD 0134+833	01:41:28.74[1]	+83:34:58.90[1]	12.88[2]	13.11[2]	DA2[2]	WD 0943+441	09:46:39.08[1]	+43:54:52.37[1]	13.19[2]	13.12[2]	DA4[2]
GJ70	01:43:20.18[6]	+04:19:17.97[6]	12.45[7]	10.92[7]	M2[12]	G43−5	09:49:51.59[9]	+06:36:35.64[9]	12.90[29]	12.48[29]	K[30]
G72−34	01:46:03.66[1]	+35:54:49.40[1]	13.84[10]	12.98[10]	K[11]	WD 0954−710	09:55:22.89[1]	−71:18:08.31[1]	13.60[2]	13.48[2]	DA4[2]
WD 0147+674	01:51:10.29[1]	+67:39:31.30[1]	14.17[2]	14.42[2]	DA2[2]	G236−30	10:28:48.37[1]	+62:59:45.00[1]	13.62[15]	12.87[15]	G5[15]
WD 0148+467	01:52:02.96[6]	+47:00:06.65[6]	12.50[2]	12.44[2]	DA3[2]	WD 1029+537	10:32:10.26[31]	+53:29:36.40[31]	14.18[2]	14.46[2]	DA1[2]
WD 0204−306*	02:07:02.28[1]	−30:23:32.20[1]	–	16.18[13]	DA[2]	WD 1031−114	10:33:42.76[25]	−11:41:38.35[25]	12.85[2]	13.03[2]	DA2[2]
LP 885−23*	02:07:06.33[1]	−30:24:22.90[1]	–	13.06[13]	M0[13]	WD 1034+001	10:37:03.81[1]	−00:08:19.30[1]	12.86[32]	13.23[32]	DOZ1[2]
WD 0214+568	02:17:33.52[1]	+57:06:47.50[1]	13.56[2]	13.68[2]	DA2[2]	WD 1041+580	10:44:46.10[33]	+57:44:35.00[33]	14.37[2]	14.60[2]	DA1[2]
WD 0227+050	02:30:16.62[6]	+05:15:50.68[6]	12.75[7]	12.80[7]	DA3[2]	WD 1053−550	10:55:13.54[1]	−55:19:05.20[1]	14.42[2]	14.32[2]	DA4[2]
WD 0302+621	03:06:16.69[1]	+62:22:22.68[1]	15.17[2]	14.95[2]	DA4/6[2]	WD 1056−384	10:58:20.11[1]	−38:44:25.10[1]	13.86[34]	14.05[34]	DA2[2]
WD 0316−849	03:09:59.89[14]	−84:43:21.14[14]	11.62[14]	10.55[14]	DAH[2]	G146−76	10:59:57.48[9]	+44:46:43.75[9]	11.15[9]	10.47[9]	G/K [20]
G174−44	03:17:23.31[1]	+52:17:42.40[1]	14.49[15]	13.75[15]	K0[16]	WD 1104+602	11:07:42.80[1]	+59:58:29.90[1]	13.78[2]	13.80[2]	DA3[2]
HG7−15	03:48:11.86[6]	+07:08:46.47[6]	12.11[29]	10.65[29]	M1[58]	WD 1105−048	11:07:59.95[1]	−05:09:25.90[1]	13.09[32]	13.06[32]	DA3[2]
WD 0435−088	04:37:47.42[17]	−08:49:10.70[17]	14.10[2]	13.77[2]	DQ7[2]	G10−4	11:10:60.00[6]	+06:25:11.51[6]	12.13[35]	11.41[35]	K[20]
WD 0446−789	04:43:46.47[1]	−78:51:50.40[1]	13.36[2]	13.47[2]	DA3[2]	G254−24	11:32:23.31[6]	+76:39:18.03[6]	12.18[36]	11.53[36]	G0[16]
WD 0447+176	04:50:13.52[6]	+17:42:06.21[6]	12.63[17]	12.65[18]	sdO[19]	WD 1134+300	11:37:05.10[6]	+29:47:58.34[6]	12.41[34]	12.49[34]	DA2[2]
WD 0455−282	04:57:13.90[2]	−28:07:54.00[2]	13.63[2]	13.95[2]	DA1[2]	SDSS 09310	11:38:02.62[3]	+57:29:23.89[3]	15.24[4]	14.99[4]	A0/F3[5]
WD 0501−289	05:03:55.51[2]	−28:54:34.57[2]	13.55[2]	13.90[2]	DO[2]	G10−54	11:49:48.20[1]	+06:08:52.14[1]	13.17[37]	12.57[37]	G[20]
G191−52	05:44:43.55[1]	+56:15:30.80[1]	14.02[15]	13.26[15]	G[20]	WD 1153−484	11:56:11.43[1]	−48:40:03.18[1]	12.65[2]	12.85[2]	DA2[2]
U1050−027792	05:52:18.18[1]	+15:51:52.70[1]	14.42[21]	13.70[21]	–	WD 1210+533	12:13:24.64[1]	+53:03:57.36[1]	13.78[2]	14.12[2]	DAO1[2]
WD 0552−041	05:55:09.53[17]	−04:10:07.10[17]	15.50[2]	14.45[2]	DC/DZ[2]	WD 1211−169	12:14:10.53[14]	−17:14:20.19[14]	11.04[15]	10.13[15]	DAH[2]
HD 270422	05:56:47.74[14]	−66:39:05.27[14]	10.92[9]	10.05[9]	G0[22]	GJ459.3	12:19:24.09[6]	+28:22:56.52[6]	12.06[26]	10.62[26]	M2[26]
HD 270477	05:59:33.36[14]	−67:01:13.72[14]	10.73[9]	10.28[9]	F8[22]	SDSS 12720	12:22:41.66[3]	+42:24:43.66[3]	15.18[4]	15.04[4]	A0/F2[5]
HD 271747	05:59:58.62[9]	−66:06:08.91[9]	11.82[9]	11.29[9]	G0[22]	WD 1223−659	12:26:42.02[1]	−66:12:18.70[1]	14.37[2]	13.97[2]	DA7[2]
WD 1234+481	12:36:45.18[1]	+47:55:22.34[1]	14.09[2]	14.42[2]	DA1[2]	WD 2047+372	20:49:06.69[1]	+37:28:13.90[1]	13.07[2]	12.93[2]	DA3[2]
SA 104−428	12:41:41.28[1]	−00:26:26.20[1]	13.58[32]	12.63[32]	G8[38]	WD 2111+498	21:12:44.05[1]	+50:06:17.80[1]	12.84[2]	13.08[2]	DA1[2]
SA 104−490	12:44:33.46[1]	−00:25:51.70[1]	13.07[32]	12.57[32]	G3[39]	WD 2105−820	21:13:13.90[2]	−81:49:04.00[2]	13.82[2]	13.61[2]	DA5[2]
G14−24	13:02:01.58[1]	−02:05:21.42[1]	13.52[27]	12.81[27]	K0[20]	WD 2111+261	21:13:45.93[1]	+26:21:33.20[1]	14.92[2]	14.68[2]	DA6[2]
GJ2097	13:07:04.31[25]	+20:48:38.54[25]	14.10[40]	12.54[40]	M1[12]	WD 2117+539	21:18:56.27[9]	+54:12:41.25[9]	12.40[2]	12.33[2]	DA3[2]
SDSS 08393	13:10:32.07[3]	+54:18:33.66[3]	15.30[4]	15.08[4]	A0/F3[5]	WD 2115−560	21:19:36.52[1]	−55:50:14.20[1]	14.43[2]	14.28[2]	DAZ5[2]
GJ507.1	13:19:40.13[6]	+33:20:47.49[6]	12.10[29]	10.57[29]	M2[12]	WD 2122+282	21:24:58.30[2]	+28:26:05.00[2]	13.80[2]	14.00[2]	DA0[55]
WD 1319+466	13:21:15.08[1]	+46:23:23.68[1]	14.55[2]	14.55[2]	DA3[2]	WD 2136+828	21:33:43.25[1]	+83:03:32.40[1]	13.01[2]	13.02[1]	DA3[2]
WD 1323−514	13:26:09.65[1]	−51:41:35.78[1]	14.60[2]	14.60[2]	DA2[2]	WD 2134+218	21:36:36.30[2]	+22:04:33.00[2]	14.41[2]	14.45[2]	DA3[2]
WD 1327−083	13:30:13.64[6]	−08:34:29.49[6]	12.40[7]	12.34[7]	DA4[2]	WD 2140+207	21:42:42.00[1]	+20:59:58.24[1]	13.40[2]	13.24[2]	DQ6[2]
GJ521	13:39:24.10[6]	+46:11:11.37[6]	11.50[9]	10.26[9]	M2[12]	WD 2147+280	21:49:54.53[1]	+28:16:59.80[1]	14.66[2]	14.68[2]	DB4[2]

Table 4 – *continued*

Star	RA (J2000) (hh:mm:ss)	Dec. (J2000) (dd:pp:ss)	*B* (mag)	*V* (mag)	Type	Star	RA (J2000) (hh:mm:ss)	Dec. (J2000) (dd:pp:ss)	*B* (mag)	*V* (mag)	Type
WD 1408+323	14:10:26.95[1]	+32:08:36.10[1]	13.96[2]	13.97[2]	DA3[2]	WD 1918+725	19:18:10.5[2]	+72:37:24.00[2]	14.70[48]	15.12[48]	DA2[2]
SDSS 09626	14:29:51.06[3]	+39:28:25.43[3]	15.23[4]	14.99[4]	A0[5]	WD 1914−598	19:18:44.84[1]	−59:46:33.80[1]	14.34[2]	14.39[2]	DA[2]
GJ570.2	14:57:32.30[6]	+31:23:44.61[6]	12.68[29]	11.54[29]	M2[12]	WD 1919+145	19:21:40.40[2]	+14:40:43.00[2]	13.07[2]	13.01[2]	DA3[2]
G15−10	15:09:46.02[6]	−04:45:06.61[6]	12.67[26]	12.01[26]	G2[41]	WD 1936+327	19:38:28.21[1]	+32:53:19.90[1]	13.46[2]	13.58[2]	DA2[2]
WD 1509+322	15:11:27.66[1]	+32:04:17.80[1]	14.20[2]	14.11[2]	DA3[2]	G23−14	19:51:49.61[6]	+05:36:45.84[6]	11.42[49]	11.02[49]	G5[26]
M5-S1490	15:17:38.64[57]	+02:02:25.60[57]	15.08[57]	14.10[57]	–	WD 2000−561.1	20:04:18.00[2]	−56:02:47.00[2]	–	15.20[50]	DA1[2]
G167−50	15:35:31.55[1]	+27:51:02.20[1]	14.25[15]	13.50[15]	G[42]	WD 2004−605	20:09:05.24[51]	−60:25:41.60[51]	13.10[2]	13.40[2]	DA1[2]
G179−54	15:46:08.25[1]	+39:14:16.40[1]	13.90[42]	13.41[42]	F[42]	WD 2014−575	20:18:54.90[52]	−57:21:34.00[52]	13.40[2]	13.70[2]	DA2[2]
G224−83	15:46:14.68[1]	+62:26:39.60[1]	13.86[15]	12.67[15]	K[42]	WD 2028+390	20:29:56.16[1]	+39:13:32.00[1]	13.22[2]	13.37[2]	DA2[2]
WD 1553+353	15:55:01.99[1]	+35:13:28.70[1]	14.64[2]	14.75[2]	DA2[2]	WD 2032+248	20:34:21.88[6]	+25:03:49.72[6]	11.47[7]	11.55[7]	DA2[2]
G16−20	15:58:18.62[9]	+02:03:06.11[9]	11.34[42]	10.75[42]	K[20]	WD 2034−532	20:38:16.84[1]	−53:04:25.40[1]	14.41[2]	14.46[2]	DB4[2]
WD 1606+422	16:08:22.20[1]	+42:05:43.20[1]	13.93[2]	13.82[2]	DA4[2]	G24−25	20:40:16.10[9]	+00:33:19.74[9]	11.23[9]	10.61[9]	G0[53]
WD 1615−154	16:17:55.26[1]	−15:35:51.90[1]	13.22[2]	13.42[2]	DA2[2]	WD 2039−202	20:42:34.75[6]	−20:04:35.95[6]	12.32[7]	12.40[7]	DA3[2]
GJ625	16:25:24.62[6]	+54:18:14.77[6]	11.80[9]	10.17[9]	M2[12]	SDSS 14511	20:42:42.40[3]	−00:34:03.71[3]	15.34[4]	15.11[4]	A0/F0[5]
G180−58	16:28:16.87[6]	+44:40:38.28[6]	11.87[29]	11.12[29]	G/K[20]	WD 2039−682	20:44:21.47[54]	−68:05:21.30[54]	13.19[2]	13.25[2]	DA3[2]
WD 1626+368	16:28:25.03[1]	+36:46:15.40[1]	14.02[2]	13.83[2]	DZA6[2]	SDSS 15724	20:47:38.19[3]	−06:32:13.11[3]	15.06[4]	14.87[4]	A0/F2[5]
WD 1637+335	16:39:27.83[25]	+33:25:22.30[25]	14.85[2]	14.65[2]	DA5[2]	WD 2152−548	21:56:21.27[1]	−54:38:23.00[1]	13.80[2]	14.30[2]	DA1[2]
SDSS 13028	16:40:24.18[3]	+24:02:14.91[3]	15.45[4]	15.26[4]	A0[5]	GJ851	22:11:30.09[6]	+18:25:34.29[6]	11.37[7]	10.23[7]	M2[12]
WD 1659−531	17:02:56.33[43]	−53:14:36.63[43]	13.57[2]	13.47[2]	DA4[2]	WD 2211−495	22:14:11.91[9]	−49:19:27.26[9]	11.37[2]	11.71[2]	DA1[2]
G139−16	17:09:47.38[1]	+08:04:25.50[1]	13.31[24]	12.61[24]	K[20]	WD 2216−657	22:19:48.35[1]	−65:29:18.11[1]	14.57[2]	14.43[2]	DZ5[2]
G170−47	17:32:41.63[6]	+23:44:11.64[6]	9.54[9]	8.94[9]	G0[28]	GJ863	22:33:02.23[6]	+09:22:40.70[6]	11.91[7]	10.74[7]	M0[12]
2MASS J175713	17:57:13.25[1]	+67:03:40.90[1]	11.91[1]	12.01[1]	A3[44]	SDSS 14276	22:42:04.17[3]	+13:20:28.61[3]	14.48[4]	14.32[4]	A0[5]
TYC 4213−617	18:00:02.14[14]	+66:45:54.96[14]	11.24[9]	10.68[9]	–	WD 2251−634	22:55:10.00[2]	−63:10:27.00[2]	–	14.28[2]	DA[2]
BD +661071	18:02:10.92[14]	+66:12:26.39[14]	10.93[9]	10.52[9]	F5[42]	WD 2309+105	23:12:21.62[25]	+10:47:04.25[25]	12.78[32]	13.09[32]	DA1[2]
G184−17	18:40:29.27[1]	+19:36:06.65[1]	14.90[27]	14.08[27]	K[20]	G190−15	23:13:38.82[6]	+39:25:02.59[6]	11.57[29]	10.98[29]	F6[28]
WD 1837−619	18:42:29.73[45]	−61:51:45.10[45]	15.01[2]	14.90[2]	DC5[2]	SDSS 00832	23:30:24.90[3]	−00:09:34.90[3]	15.15[4]	14.99[4]	A0[5]
G184−20	18:43:52.50[1]	+16:00:34.20[1]	13.37[46]	12.61[47]	G[20]	WD 2329+407	23:31:35.65[1]	+41:01:30.70[1]	13.85[2]	13.82[2]	DA3[2]
WD 1845+019	18:47:39.08[1]	+01:57:35.62[1]	12.73[2]	12.95[2]	DA2[2]	WD 2331−475	23:34:02.20[1]	−47:14:26.50[1]	13.15[3]	13.44[2]	DA1[2]
WD 1900+705	19:00:10.25[1]	+70:39:51.24[1]	13.24[2]	13.19[2]	DAP4[9]	G241−64	23:41:24.49[1]	+59:24:34.90[1]	13.45[15]	12.70[15]	K[20]
GJ745A	19:07:05.56[6]	+20:53:16.97[6]	12.40[7]	10.77[7]	M2[12]	G171−15	23:45:02.71[9]	+44:40:03.60[9]	12.00[9]	11.75[9]	G0[56]
GJ745B	19:07:13.20[6]	+20:52:37.24[6]	12.38[7]	10.77[7]	M2[12]	WD 2352+401	23:54:56.25[1]	+40:27:30.10[1]	15.13[2]	14.94[2]	DQ6[2]

[1]2MASS survey (Cutri et al. 2003); [2]McCook & Sion (1999) compilation and online updates; [3]SDSS seventh data release (Abazajian et al. 2009); [4]SDSS, derived with the SEGUE pipeline (Lee et al. 2008) and the transformations by Lupton (2005); [5]SDSS, derived with the SEGUE pipeline (Lee et al. 2008); [6]van Leeuwen (2007); [7]Koen et al. (2010); [8]Gray et al. (2006); [9]Tycho-2 catalogue of bright sources (Høg et al. 2000); [10]Carney & Latham (1987); [11]from $T_{\rm eff}$ by Laird, Carney & Latham (1988); [12]Jenkins et al. (2009); [13]Garcés, Catalán & Ribas (2011); [14]Hog et al. (1998), for approximate Johnson magnitudes the formulae $V = {\rm VT} - 0.090({\rm BT} - {\rm VT})$ and $B - V = 0.850({\rm BT} - {\rm VT})$ were used; [15]Kharchenko (2001); [16]Bidelman (1985); [17]Salim & Gould (2003); [18]'Subdwarf database' (Østensen 2006); [19]misclassified as a WD by McCook & Sion (1999) according to Stroeer et al. (2007); [20]from $T_{\rm eff}$ by Carney et al. (1994); [21]Galadí-Enríquez, Trullols & Jordi (2000)); [22]Henry Draper Catalogue (Cannon & Pickering 1993); [23]Caballero & Solano (2007); [24]Carney et al. (1994); [25]UCAC3 (Zacharias et al. 2009); [26]*Hipparcos* input catalogue (Turon, Hilditch & Hilditch 1993); [27]Marshall (2007); [28]Cenarro et al. (2007); [29]Lépine & Shara (2005); [30]from $T_{\rm eff}$ by Latham et al. (2002); [31]Bicay et al. (2000); [32]Landolt (1992); [33]Zickgraf et al. (2003); [34]Landolt & Uomoto (2007); [35]Giclas, Burnham & Thomas (1971); [36]Ivanov (2008); [37]Mermilliod (1994); [38]Buscombe & Foster (1995); [39]Drilling & Landolt (1979); [40]Pesch (1976); [41]van Altena, Lee & Hoffleit (1995); [42]Kharchenko & Roeser (2009); [43]7th SDSS photometric data release (Adelman-McCarthy et al. 2009); [44]Tanabé et al. (2008); [45]Downes et al. (2001); [46]Monet et al. (2003); [47]Zapatero Osorio & Martín (2004); [48]Greenstein (1984); [49]Zacharias et al. (2005); [50]Malina et al. (1994); [51]Fleming et al. (1996); [52]Koester et al. (2001); [53]Roeser & Bastian (1988); [54]Wegner (1973); [55]Vennes, Korpela & Bowyer (1997); [56]Lee (1984); [57]Stetson standard in M5 (Stetson 2000); data available at http://cadcwww.dao.nrc.ca/community/STETSON/standards; [58]Endl et al. (2006); *possible identification problem, see also Section 6.1.

literature information are stored locally and can be accessed upon request.

ACKNOWLEDGMENTS

We would like to acknowledge the support of the Istituto Nazionale di Astrofisica (INAF) and specifically of the Bologna Observatory; we also acknowledge support of the ASI (Agenzia Spaziale Italiana) under contracts to INAF I/037/08/0 and I/058/10/0, dedicated to the *Gaia* mission, and the Italian participation to DPAC. This work was supported by the MICINN (Spanish Ministry of Science and Innovation) – FEDER through grant AYA2009-14648-C02-01 and CONSOLIDER CSD2007-00050. EP acknowledges the hospitality of the ASDC (ASI Science Data Center), where part of this work was carried out. We warmly thank the technical staff of the San Pedro Mártir, Calar Alto, Loiano, La Silla NTT and REM, and Roque de Los Muchachos TNG observatories.

We made use of the following softwares and online data bases (in alphabetical order): 2MASS, CALSPEC, CataXcorr, ESO-DSS, ESO Skycat tool, iraf, Kawka web page, MILES, NGSL, SAOImage DS9, SDSS and SEGUE, SExtractor, SIMBAD, SuperMongo, UCAC3, USNO catalogues, Villanova White Dwarf Catalogue. We thank G. S. Aldering, M. A. Barstow, M. E. Kayser and A. Korn for sharing their information with us. We also thank M. Bessell, who was the referee of this paper and provided extremely useful comments not only to improve the paper, but for the whole project.

The survey presented in this paper relies on data obtained at ESO (proposals 182.D-0287, 086.D-0176, 087.D-0213 and

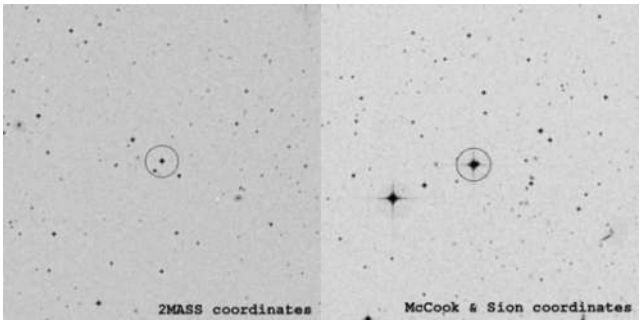

Figure 7. The unsolved case of WD 1148−230. The finding chart on the left shows the star that in SIMBAD is associated with WD 1148−230, at the coordinates reported by 2MASS (Cutri et al. 2003), and the one on the right the star corresponding to the WD 1148−230, coordinates by McCook & Sion (1999) and Stys et al. (2000). Both images are 10 arcmin wide, north is up and east is left.

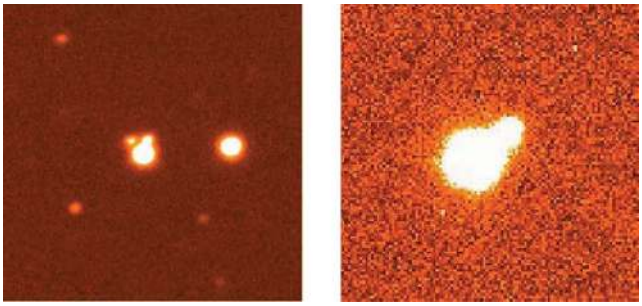

Figure 8. Image cut-out of candidate WD 0406+592 (left-hand panel) observed with DOLoRes@TNG in the *R* band, showing two close companions; similarly, a cut-out of candidate WD 2058+181 (right-hand panel), observed in San Pedro Mártir in the *R* band, shows a close companion.

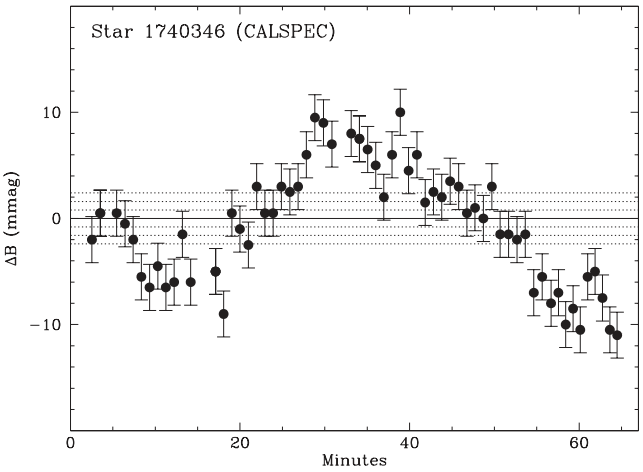

Figure 9. Our best light curve for the CALSPEC standard 1740346 (obtained with BFOSC in Loiano on 2010 September 1), originally one of our *primary SPSS* candidates. The average of all field stars' magnitude differences (i.e. zero) is marked with a solid line, while the $\pm 1\sigma$, 2σ and 3σ variations are marked with dotted lines.

089.D-0077), Calar Alto (proposals H07-2.2-024, F08-2.2-043, H08-2.2-041, F10-2.2-027, H10-2.2-042, H10-2.2-042 and F12-2.2-034), TNG (proposals AOT16_37, AOT17_3, AOT18_14, AOT19_14, AOT20_41 and AOT21_1), Loiano (10 accepted proposals starting from 2007 June), San Pedro Mártir (seven accepted proposals starting from 2007 October) and REM (proposals AOT16_16012, AOT17_17012, AOT18_18002, AOT19_19010, AOT20_78, AOT21_2, AOT22_18, AOT23_7 and AOT24_21).

REFERENCES

Abazajian K. N. et al., 2009, ApJS, 182, 543
Adelman-McCarthy J. K. et al., 2009, VizieR Online Data Catalog, 2294, 0
Altavilla G., Federici L., Pancino E., Bragaglia A., Bellazzini M., Cacciari C., 2008, Gaia Technical Report No. GAIA-C5-TN-OABO-GA-002
Altavilla G., Bragaglia A., Pancino E., Bellazzini M., Cacciari C., Federici L., Ragaini S., 2010a, Gaia Technical Report No. GAIA-C5-TN-OABO-GA-001
Altavilla G., Bragaglia A., Pancino E., Bellazzini M., Cacciari C., Federici L., Ragaini S., 2010b, Gaia Technical Report No. GAIA-C5-TN-OABO-GA-003
Altavilla G., Pancino E., Marinoni S., Cocozza G., Bellazzini M., Bragaglia A., Carrasco J. M. A., Federici L., 2011, Gaia Technical Report No. GAIA-C5-TN-OABO-GA-004
Altman M., Bastian U., 2009, Gaia Technical Report No. GAIA-C3-TN-ARI-MA-002
Bakos G. Á., Sahu K. C., Németh P., 2002, ApJS, 141, 187
Bellazzini M., Bragaglia A., Federici L., Diolaiti E., Cacciari C., Pancino E., 2006, Gaia Technical Report No. GAIA-C5-TN-OABO-MBZ-001
Bertin E., Arnouts S., 1996, A&AS, 117, 393
Bessell M. S., 1999, PASP, 111, 1426
Bessell M., Murphy S., 2012, PASP, 124, 140
Bica E., Bonatto C., Giovannini O., 1996, A&AS, 119, 211
Bicay M. D., Stepanian J. A., Chavushyan V. H., Erastova L. K., Ayvazyan V. T., Seal J., Kojoian G., 2000, A&AS, 147, 169
Bidelman W. P., 1985, ApJS, 59, 197
Bohlin R. C., 1996, AJ, 111, 1743
Bohlin R. C., 2007, in Sterken C., ed., ASP Conf. Ser. Vol. 364, The Future of Photometric, Spectrophotometric and Polarimetric Standardization. Astron. Soc. Pac., San Francisco, p. 315
Bohlin R. C., Cohen M., 2008, AJ, 136, 1171
Bohlin R. C., Gilliland R. L., 2004, AJ, 127, 3508
Bohlin R. C., Colina L., Finley D. S., 1995, AJ, 110, 1316
Bohlin R. C., Dickinson M. E., Calzetti D., 2001, AJ, 122, 2118
Bohlin R. C., Lindler D. J., Riess A., 2005, Space Telescope NICMOS Instrument Science Report. p. 2
Bohlin R. C. et al., 2011, AJ, 141, 173
Brown A., Jordi C., Fabricius C., van Leeuwen F., 2010, Gaia Technical Report No. GAIA-C5-TN-LEI-AB-020
Buscombe W., Foster B. E., 1995, MK Spectral Classifications. Twelfth General Catalogue, Epoch 2000 Including UBV Photometry. Northwestern University, Evanston, Illinois
Caballero J. A., Solano E., 2007, ApJ, 665, L151
Cacciari C., 2011, in EAS Publ. Ser. Vol. 45, Gaia Spectro-Photometry Absolute Calibration and Comparison to Classical Systems. p. 155
Cannon A. J., Pickering E. C., 1993, VizieR Online Data Catalog, 3135, 0
Carney B. W., Latham D. W., 1987, AJ, 93, 116
Carney B. W., Latham D. W., Laird J. B., Aguilar L. A., 1994, AJ, 107, 2240
Carrasco J. M., Jordi C., Figueras F., Anglada Escudé G., Amores E. B., 2006, Gaia Technical Report No. GAIA-C5-TN-UB-JMC-001
Carrasco J. M., Jordi C., Lopez-Marti B., Figueras F., Anglada Escudé G., 2007, Gaia Technical Report No. GAIA-C5-TN-UB-JMC-002
Casagrande L., Portinari L., Flynn C., 2006, MNRAS, 373, 13
Castanheira B. G. et al., 2007, A&A, 462, 989
Castelli F., Kurucz R. L., 2003, in Piskunov N., Weiss W. W., Gray D. F., eds, Proc. IAU Symp. 210, Modelling of Stellar Atmospheres. Astron. Soc. Pac., San Francisco, p. 20
Cenarro A. J. et al., 2007, MNRAS, 374, 664
Colina L., Bohlin R. C., 1994, AJ, 108, 1931
Crifo F., Jasniewicz G., Soubiran C., Katz D., Siebert A., Veltz L., Udry S., 2010, A&A, 524, A10
Cutri R. M. et al., 2003, The IRSA 2MASS All-Sky Point Source Catalog. NASA/IPAC Infrared Science Archive (http://irsa.ipac.caltech.edu/applications/Gator/)

Downes R. A., Webbink R. F., Shara M. M., Ritter H., Kolb U., Duerbeck H. W., 2001, PASP, 113, 764
Drilling J. S., Landolt A. U., 1979, AJ, 84, 783
Dupuis J., Vennes S., Chayer P., Hurwitz M., Bowyer S., 1998, ApJ, 500, L45
Dvorak S. W., 2004, Inf. Bull. Var. Stars, 5542, 1
Eisenstein D. J. et al., 2006, ApJS, 167, 40
Endl M., Cochran W. D., Kürster M., Paulson D. B., Wittenmyer R. A., MacQueen P. J., Tull R. G., 2006, ApJ, 649, 436
Eyer L., Grenon M., 1997, in Bonnet R. M. et al., eds, Proc. ESA Symp. 'Hipparcos – Venice '97', ESA SP-402: Photometric Variability in the HR Diagram. ESA, Noordwijk, p. 467
Eyer L., Mowlavi N., 2008, J. Phys. Conf. Ser., 118, 012010
Fabricius C. et al., 2009, Gaia Technical Report No. GAIA-C5-TN-UB-CF-012
Federici L. et al., 2006, Gaia Technical Report No. GAIA-C5-TN-OABO-LF-001
Fleming T. A., Snowden S. L., Pfeffermann E., Briel U., Greiner J., 1996, A&A, 316, 147
Galadí-Enríquez D., Trullols E., Jordi C., 2000, A&AS, 146, 169
Garcés A., Catalán S., Ribas I., 2011, A&A, 531, A7
Giclas H. L., Burnham R., Thomas N. G., 1971, Lowell Proper Motion Survey: Northern Hemisphere. Lowell Observatory, Flagstaff, Arizona
Gray R. O., Corbally C. J., Garrison R. F., McFadden M. T., Bubar E. J., McGahee C. E., O'Donoghue A. A., Knox E. R., 2006, AJ, 132, 161
Greenstein J. L., 1984, ApJ, 276, 602
Gregg M. D. et al., 2004, Am. Astron. Soc. Meeting, 205, 94.6 36, 1496
Gustafsson B., Edvardsson B., Eriksson K., Jørgensen U. G., Nordlund Å., Plez B., 2008, A&A, 486, 951
Hamuy M., Walker A. R., Suntzeff N. B., Gigoux P., Heathcote S. R., Phillips M. M., 1992, PASP, 104, 533
Hamuy M., Suntzeff N. B., Heathcote S. R., Walker A. R., Gigoux P., Phillips M. M., 1994, PASP, 106, 566
Hawarden T. G., Leggett S. K., Letawsky M. B., Ballantyne D. R., Casali M. M., 2001, MNRAS, 325, 563
Hog E., Kuzmin A., Bastian U., Fabricius C., Kuimov K., Lindegren L., Makarov V. V., Roeser S., 1998, A&A, 335, L65
Høg E. et al., 2000, A&A, 355, L27
Holberg J. B., Oswalt T. D., Sion E. M., 2002, ApJ, 571, 512
Hubeny I., Lanz T., 1995, ApJ, 439, 875
Ivanov G. A., 2008, Kinematika Fizika Nebesnykh Tel., 24, 480
Jenkins J. S., Ramsey L. W., Jones H. R. A., Pavlenko Y., Gallardo J., Barnes J. R., Pinfield D. J., 2009, ApJ, 704, 975
Jordi C., 2011, in EAS Publ. Ser. Vol. 45, Gaia Photometry: Methods, Performances and Problems. p. 149
Jordi C., Fabricius C., Figueras F., Voss H., Carrasco J. M., 2007, Gaia Technical Report No. GAIA-C5-TN-UB-CJ-042
Jordi C. et al., 2010, A&A, 523, A48
Kaiser M. E., Kruk J. W., McCandliss S. R., Sahnow D. J., Dixon W. V., Bohlin R. C., Deustua S. E., 2007, in Sterken C., ed., ASP Conf. Ser. Vol. 364, The Future of Photometric, Spectrophotometric and Polarimetric Standardization. Astron. Soc. Pac., San Francisco, p. 361
Kaiser M. E. et al., 2010, Hubble after SM4: Preparing JWST
Kawka A., Vennes S., Schmidt G. D., Wickramasinghe D. T., Koch R., 2007, ApJ, 654, 499
Kharchenko N. V., 2001, Kinematika Fizika Nebesnykh Tel., 17, 409
Kharchenko N. V., Roeser S., 2009, VizieR Online Data Catalog, 1280, 0
Kilkenny D., 2007, Commun. Asteroseismol., 150, 234
Kilkenny D., Menzies J. W., 1989, South African Astron. Obser. Circular, 13, 25
Koen C., Kilkenny D., van Wyk F., Marang F., 2010, MNRAS, 403, 1949
Koester D. et al., 2001, A&A, 378, 556
Laird J. B., Carney B. W., Latham D. W., 1988, AJ, 95, 1843
Landolt A. U., 1983, AJ, 88, 853
Landolt A. U., 1992, AJ, 104, 372
Landolt A. U., Uomoto A. K., 2007, AJ, 133, 768
Lanz T., Hubeny I., 2003, ApJS, 146, 417
Lanz T., Hubeny I., 2007, ApJS, 169, 83
Latham D. W., Stefanik R. P., Torres G., Davis R. J., Mazeh T., Carney B. W., Laird J. B., Morse J. A., 2002, AJ, 124, 1144
Lee S.-G., 1984, AJ, 89, 702
Lee Y. S. et al., 2008, AJ, 136, 2022
Lépine S., Shara M. M., 2005, AJ, 129, 1483
Lupton R., 2005, http://www.sdss.org/dr7/algorithms/sdssUBVRITransform.html#Lupton2005
Luyten W. J., 1957, AJ, 62, 339
McCook G. P., Sion E. M., 1999, ApJS, 121, 1
Malina R. F. et al., 1994, AJ, 107, 751
Marinoni S., 2011, PhD thesis, Bologna University
Marinoni S., Pancino E., Altavilla G., Cocozza G., Carrasco J. M., Monguio M., Villardell F., 2012, Gaia Technical Report No. GAIA-C5-TN-OABO-SMR-001
Marshall J. L., 2007, AJ, 134, 778
Mermilliod J.-C., 1994, VizieR Online Data Catalog, 2193, 0
Mignard F., 2005, in Seidelmann P. K., Monet A. K. B., eds, ASP Conf. Ser. Vol. 338, Astrometry in the Age of the Next Generation of Large Telescopes. Astron. Soc. Pac., San Francisco, p. 15
Monet D. G. et al., 2003, AJ, 125, 984
Montegriffo P., 2011, Gaia Technical Report No. GAIA-C5-TN-OABO-PMN-006
Montegriffo P., Bellazzini M., 2009, Gaia Technical Report No. GAIA-C5-TN-OABO-PMN-003
Montegriffo P., Carrasco J. M., Jordi C., Fabricius C., Cacciari C., 2011, Gaia Technical Report No. GAIA-C5-TN-OABO-PMN-005
Oke J. B., 1990, AJ, 99, 1621
Østensen R. H., 2006, Balt. Astron., 15, 85
Østensen R. H. et al., 2010, A&A, 513, A6
Oswalt T. D., Hintzen P. M., Luyten W. J., 1988, ApJS, 66, 391
Pakštiene E., Solheim J.-E., 2003, Balt. Astron., 12, 221
Pancino E., 2010, preprint (arXiv:1009.1748)
Pancino E., Altavilla G., Bellazzini M., Marinoni S., Bragaglia A., Federici L., Cacciari C., 2008, Gaia Technical Report No. GAIA-C5-TN-OABO-EP-001
Pancino E. et al., 2009, Gaia Technical Report No. GAIA-C5-TN-OABO-EP-003
Pancino E., Altavilla G., Carrasco J. M., Marinoni S., Cocozza G., Bellazzini M., Federici L., 2011, Gaia Technical Report No. GAIA-C5-TN-OABO-EP-006
Pasquier J.-F., 2011, in EAS Publ. Ser. Vol. 45, Native and Irradiated Charge Transfer Inefficiency Characterization. p. 61
Perryman M. A. C. et al., 1997, A&A, 323, L49
Pesch P., 1976, AJ, 81, 1117
Pokorny R. S., Jones H. R. A., Hambly N. C., 2003, A&A, 397, 575
Prod'Homme T., 2011, in EAS Publ. Ser. Vol. 45. Radiation Effects on Gaia CCDs, Modelling to Mitigate the Threat. p. 55
Ragaini S., Bellazzini M., Montegriffo P., Cacciari C., 2009a, Gaia Technical Report No. GAIA-C5-TN-OABO-SR-001
Ragaini S., Montegriffo P., Bellazzini M., Cacciari C., 2009b, Gaia Technical Report No. GAIA-C5-TN-OABO-SR-002
Rauch T., Deetjen J. L., 2003, in Hubeny I., Mihalas D., Werner K., eds, ASP Conf. Ser. Vol. 288, Stellar Atmosphere Modeling. Astron. Soc. Pac., San Francisco, p. 103
Reach W. T. et al., 2005, PASP, 117, 978
Reid I. N., 1996, AJ, 111, 2000
Ringat E., 2012, in Kilkenny D., Jeffery C. S., Koen C., eds, ASP Conf. Ser. Vol. 452, Fifth Meeting on Hot Subdwarf Stars and Related Objects. Astron. Soc. Pac., San Francisco, p. 99
Roeser S., Bastian U., 1988, A&AS, 74, 449
Salim S., Gould A., 2003, ApJ, 582, 1011
Sánchez S. F., Aceituno J., Thiele U., Pérez-Ramírez D., Alves J., 2007, PASP, 119, 1186
Sánchez-Blázquez P. et al., 2006, MNRAS, 371, 703
Sembach K. R., Savage B. D., 1992, ApJS, 83, 147
Silvestri N. M., Oswalt T. D., Hawley S. L., 2002, AJ, 124, 1118

Sion E. M., Holberg J. B., Oswalt T. D., McCook G. P., Wasatonic R., 2009, AJ, 138, 1681
Sordo R., Munari U., 2006, A&A, 452, 735
Sordo R. et al., 2010, Ap&SS, 328, 331
Stetson P. B., 2000, PASP, 112, 925
Stone R. P. S., 1977, ApJ, 218, 767
Stone R. P. S., Baldwin J. A., 1983, MNRAS, 204, 347
Stritzinger M., Suntzeff N. B., Hamuy M., Challis P., Demarco R., Germany L., Soderberg A. M., 2005, PASP, 117, 810
Stroeer A., Heber U., Lisker T., Napiwotzki R., Dreizler S., Christlieb N., Reimers D., 2007, A&A, 462, 269
Stys D. et al., 2000, PASP, 112, 354
Tanabé, et al., 2008, PASJ, 60, 375
Trager S., 2010, Gaia Technical Report No. GAIA-C5-TN-UG-ST-002
Tsalmantza P., Bailer-Jones C. A. L., 2009, Gaia Technical Report No. GAIA-C8-TN-MPIA-PAT-004
Tsalmantza P. et al., 2012, A&A, 537, A42
Turnshek D. A., Bohlin R. C., Williamson R. L., II, Lupie O. L., Koornneef J., Morgan D. H., 1990, AJ, 99, 1243
Turon C., Hilditch R., Hilditch R., 1993, The Observatory, 113, 223
van Altena W. F., Lee J. T., Hoffleit D., 1995, VizieR Online Data Catalog, 1174, 0
van Leeuwen F., 2007, A&A, 474, 653
van Leeuwen F., Pancino E., Altavilla G., 2011, Gaia Technical Report No. GAIA-C5-SP IOA-FVL-072
Vennes S., Korpela E., Bowyer S., 1997, AJ, 114, 1567
Wegner G., 1973, MNRAS, 163, 381
Weiler M., Babusiaux C., Short A., 2011, EAS Publ. Ser. Vol. 45, Implementation of Models for Charge Transfer Inefficiency (CTI) in the Gaia Pixel-Level Data Simulator. p. 67
Yanny B. et al., 2009, AJ, 137, 4377
Zacharias N., Monet D. G., Levine S. E., Urban S. E., Gaume R., Wycoff G. L., 2005, yCat, 1297, 0
Zacharias N. et al., 2009, VizieR Online Data Catalog, 1315, 0
Zapatero Osorio M. R., Martín E. L., 2004, A&A, 419, 167
Zechmeister M., Kürster M., Endl M., 2009, A&A, 505, 859
Zickgraf F.-J., Engels D., Hagen H.-J., Reimers D., Voges W., 2003, A&A, 406, 535

This paper has been typeset from a TEX/LATEX file prepared by the author.